Physics – Uspekhi **64** (10) 967 – 989 (2021)

REVIEWS OF TOPICAL PROBLEMS PACS numbers: **95.10.–a**, 97.10.Wn, 98.62.Js

Hypervelocity stars: theory and observations

A V Tutukov, G N Dryomova, V V Dryomov

DOI: https://doi.org/10.3367/UFNe.2020.11.038892

Contents

1. Introduction **968**

2. Stars with anomalous kinematics **969**

2.1 'Flying' and 'runaway' stars: early observations and interpretations; 2.2 Prediction of hypervelocity stars. Hills scenario in the classical three-body problem; 2.3 Alternative scenarios for the generation of hypervelocity stars; 2.4 Modified Hills scenario. Prediction of stars with relativistic velocities; 2.5 Classification of stars with anomalous kinematics

3. Numerical modeling of Hills scenario **972**

3.1 Analysis of the velocity spectrum in the classical Hills scenario. Three-body problem; 3.2 Survival criteria of stars ejected from the SMBH vicinity. *N*-body problem; 3.3 Dynamical model of capture of a binary star into the SMBH vicinity; 3.4 Calculated population of S-stars in the Galaxy; 3.5 Formation probability of hypervelocity stars in the Galaxy; 3.6 Modeling of stars with relativistic velocities; 3.7 Formation probability of relativistic velocity stars in the Universe

4. Discovery of S-stars **982**

4.1 Early evidence of a supermassive black hole in the Galactic Center; 4.2 Projects of long-term monitoring of the Galactic Center. Methods of observations; 4.3 First orbit of the star S2. Progress in the study of S-stars; 4.4 Prospects for GR testing in the strong gravity regime; 4.5 Direct confirmation of the supermassive black hole in the Galactic Center

5. Discovery of hypervelocity stars **984**

5.1 History of the first HVS discovery; 5.2 Method of survey searches in photometric catalogs; 5.3 MMT-catalog of hypervelocity stars; 5.4 Gaia space telescope and the open catalog of hypervelocity stars; 5.5 Problem of central ejection confirmation

6. Searches for stars with relativistic velocities. Potential of modern astrometry **986**

6.1 Search methods; 6.2 Future space missions; 6.3 Stars with relativistic velocities as tracers of cosmological distances

7. Conclusion **988**

References **988**

Abstract. Relativistic velocity is a kinematic feature of micro-objects (elementary particles). Their application to macro objects (stars, planets, asteroids, neutron stars, and stellar-mass black holes) is currently under scientific discussion. This potential was recognized after Warren Brown discovered hypervelocity stars (HVSs) at the beginning of the 21st century. Jack Hills predicted these stars in 1988 due to the dynamical capture of a binary star by the central supermassive black hole (SMBH). The acceleration mechanism due to momentum exchange in the classical three-body problem provides the kinetic resource for HVS formation by the gravitational capture of the remaining component. The present threshold of the anomalous stellar kinematics exceeds $\sim$1700 km s^{-1} and can be reproduced by some mechanisms as alternatives to Hills's scenario. HVSs can arise due to the collisional evolution of stellar clusters, supernova explosions in close binary stars, the orbital instability of triple stars, stellar captures from other galaxies, etc. Scenarios with the participation of black holes with masses ranging from stellar values to several billion solar masses are the most promising for the generation of anomalously high stellar velocities. Hills's scenario has a special place in HVS studies, because, being based on the accidental capture of a binary star by the SMBH, it does not relate to the problem of the Galactic Center population. This scenario predicts self-consistent statistics of HVSs and captured stars which may be identified with S-stars. The discovery of S-stars played an essential role in studies of the Galactic Center; their dynamics have independently provided incontestable proof of the SMBH's existence. This review briefly discusses the history of the discovery and investigation of HVSs and S-stars, provides an account of their observational statistics, and describes their modeling methods in the classical three-body and *N* body problems. We study the limits of the effective acceleration of stars in the classical Hills scenario and the modified mechanism that allows a change of one of the

A V Tutukov [1, a], **G N Dryomova** [2, b], **V V Dryomov** [2, c]
[1] Institute of Astronomy, Russian Academy of Sciences, ul. Pyatnitskaya 48, 119017 Moscow, Russian Federation
[2] Russian Federal Nuclear Centre "Zababakhin All-Russia Research Institute of Technical Physics", ul. Vasil'eva 13, 456770 Snezhinsk, Chelyabinsk region, Russian Federation
E-mail: [a]atutukov@inasan.ru, [b] G.N.Dryomova@mail.ru, [c] V.V.Dryomov@vniitf.ru

Received 20 July 2020, revised 19 November 2020
Uspekhi Fizicheskikh Nauk **191** (10) 1017 – 1043 (2021)
Translated by P Konstantinov

binary components to another SMBH. The acceleration acquired by the star in a mutual field of two SMBHs can produce stars with relativistic velocities ($1/2\,c - 2/3\,c$). Using a self-consistent probabilistic model combining the classical and modified Hills scenarios, we predict the formation probability of HVSs in the Galaxy and of extragalactic stars with relativistic velocities. We discuss the prospects of searches for stars and asteroids with relativistic velocities by future space missions and using new knowledge about the Universe.

Keywords: kinematic anomaly, dynamical capture, Hills's scenario, S-stars, hypervelocity stars, stars with relativistic velocities, supermassive black hole, galaxies

1. Introduction

The contours of the modern kinematic model of the Galaxy appeared in the 1920s during the Great Debate between Harlow Shapley and Heber Curtis [1, 2] about the size of our Galaxy. The asymmetry in stellar motions found earlier by Jacobus Kapteyn [3] was logically explained in Bertil Lindblad's and Jan Oort's model of the differential rotation of the Galaxy [4, 5]. As a result, stellar subsystems (disk and halo) with different kinematic properties and, as later noted by Baade [6], types of stellar populations, were singled out. By the mid-20th century, a quite self-consistent kinematic model of the Galaxy was established. The model naturally included structures added later: 'thick' and 'thin' disks, a bulge, and spiral arms. But the model was not finalized because there remained objects not fit into the 'organized' kinematics, which were separated into a special class of stars with anomalous kinematics. In the course of their study, their nature turned out to be much richer than initially assumed, which required a separate classification.

Initially, two classes of rapidly moving stars with a velocity several times as high as the peculiar velocity of stars in the solar neighbors were singled out. The nature of the kinematic anomaly of objects from the first class was related to the apparent accelerated motion of stars of one sub-system (actually, the slowly rotating halo) relative to another (the rapidly rotating disk). The kinematic anomaly of objects from the second class was explained by real physical acceleration from the disruption of binary stars due to the explosion of one binary component as a type SN1b/c supernova. This idea was first put forward by Fritz Zwicky [7] and later supported by many observations [8, 9].

Other classes of stars with anomalous kinematics were predicted, and, here, the enigma of the invisible mass in the central parts of our Galaxy played a crucial role. Since the mid-1970s, numerous pieces of evidence for the concentration of dark matter in the Galactic Center have been obtained, in particular, from the analysis of the radial velocity of ionized gas showing a 'mini-spiral'-like motion [10], as well as from spectroscopic studies of CO line absorption in stars located within a one-tenth parsec central region [11]. The monitoring of a small group of fast-moving stars in the Galactic Center also suggested the presence of an invisible object with a mass of several million solar masses near the radio source Sgr A* [12].

In the 1980s, it was unknown whether the central object was a collection of dark remnants of the stellar evolution or a single object, for example, a supermassive black hole (SMBH). Exactly at that time, the idea of searching for indirect confirmation of the central invisible object arose. Jack Hills proposed and justified by calculations the scenario of the dynamical capture of a binary star by the central SMBH in the classical three-body problem [13]. During the momentum redistribution, the regrouping of the binary system by substituting one of its components by the SMBH is possible, and the second stellar component can be ejected with a velocity of several thousand km s^{-1}. The discovery of such stars, dubbed by Hills hypervelocity stars (HVSs), could be evidence of the existence of an SMBH in the Galactic Center.

But history goes its own way, and, in 2002, the captured components of binary stars, or S-stars [14], were discovered. They were named after the letter 's' in the word 'arcsecond', referring to S-stars being confined within a one-arcsecond region centered in the radio source Sgr A*. The first supervelocity star with a heliocentric velocity of ~ 850 km s^{-1} was discovered by Brown et al. in 2005 [15] in a study not directly related to searches for HVSs.

The accidental character of the discovery raised new interest in the problem of anomalous kinematics, which turned out to be underexplored. Computer laboratories of that time produced a wealth of numerical calculations modeling different scenarios of HVS formation, including the disruption of a binary system during a supernova explosion, the tidal disruption of a dwarf galaxy passing close to the Galactic Center, the dynamical evolution of a thin disk around an SMBH, the dynamical capture of binary stars and stellar clusters by the SMBH gravitational field, and, actually, the Hills scenario [16–26].

All these scenarios can produce ejections of stars with a space velocity of the order of several hundred or even a thousand km s^{-1}, which can exceed the Galactic escape velocity at the given point of observations. This property corresponds to the definition of an HVS as an object with positive binding energy with the Galaxy. For our Galactic Center, the second cosmic velocity, according to Wu et al. [27], who studied the distribution of the circular and escape velocities with the galactocentric distance, is ~ 750 km s^{-1}. In the solar vicinity, the escape velocity is ~ 500 km s^{-1}, and in the halo, at a distance of 100 kpc, it is 250–300 km s^{-1}. These estimates improve in further studies of Galactic dark matter.

Thus, searches for mechanisms of the efficient acceleration of stars became timely. Here, especially interesting are scenarios in which black holes with masses ranging from stellar values to several billion solar masses play the key role, for example, the 'kick'-scenario of stellar impact scattering on a cluster of stellar-mass black holes which, by falling towards the central SMBH, pull the stars by rejecting them back with typical HVS velocities [28]. The *in-spiral* scenario considers the plunge of a $10^3 - 10^4 M_\odot$ black hole to the Galactic Center populated with a young stellar cluster [29]. The dynamical friction arising here [30] leads to the ejection of stars with velocities of several thousand km s^{-1}. Despite the reproduction of the observed HVS velocities, these scenarios disagree with observations of the Galactic Center by requiring rich nuclear stellar clusters inside the central milliparsec (1 mpc) [31].

The Hills scenario, which is based on the accidental capture of a binary star by the SMBH, can explain the Galactic Center population [31–33] and provides components for the scenario 'binary star and SMBH', whose existence is proved [34]. Another intriguing feature is the consistency of statistics of HVS and S-stars, which could be components of one parent binary star, which is a separate topic.

By now, Buber et al. [35] have produced an open version of the HVS catalog (41 HVS), including mainly the stars discovered by Brown et al. [36]. The statistical study of HVSs enabled generalizing their properties and analyzing their spatial distribution, which proved to be anisotropic [37]. This feature is relaxed in the scenario of the pericentric approach of a young stellar cluster to the SMBH, which provides the outburst character of HVS generation and 'traces' the tangential to the cluster orbital motion [38]. The statistics on discovered HVSs are in good agreement with their birthrate as predicted by the Hills mechanism, about one star every million years [13]. This group of stars is now used as the learning matrix in the artificial neuron network for recognizing objects in big data, for example, in the Gaia catalogs [39].

The space velocity of known HVSs exceeds 1700 km s^{-1} [40], whereas theoretical estimates and model calculations show that the Hills scenario can produce dynamical ejections with velocities up to $0.1\,c$ [26]. However, this is not a kinematic limit: a change to one of the binary components by another SMBH in the kinematic Hills scenario enables relativistic ejections due to momenta redistributions in the three-body problem [41, 42]. Although the birth of stars with relativistic velocities in our Galaxy is impossible because of the single central SMBH, which is firmly established from Keplerian orbits of S-stars [43], their appearance there is not ruled out. Numerous examples of merging galaxies [44] with central parts hosting SMBHs illustrate the possibility of a modified Hills scenario that can give rise to stars with relativistic velocities [41, 42].

So far, this is a hypothetical class of stars with anomalous kinematics. The physical justification of the existence of such objects and probabilistic estimates of their abundance [45] give hope that they will be discovered in the near future. To do this, the astrometric barrier related to the photometric and spectroscopic registration of solar-type stars at distances of tens and hundreds of megaparsecs should be overcome. The present review is particularly devoted to answering the question of how ready we are to welcome this discovery.

The structure of this review is as follows. Section 2 provides a historical retrospect of the discovery of 'flying' stars and briefly describes the conceptual basis of the modern classification of stars with anomalous kinematics. Section 3 describes the methods and results of numerical modeling of the classical and modified Hills scenarios in the three-body and N-body problem setup. We present the probabilistic approach to numerical calculations, enabling us to estimate the generation probabilities of S-stars and HVSs in our Galaxy, formulate their survival criteria, and analyze the calculated velocity spectra to justify the limiting space velocities stars. Section 4 is devoted to the discovery of S-stars and long-term monitoring of the Galactic Center. Here, we provide a complete list of direct and indirect confirmations of the presence of an SMBH near the location of the radio source Sgr A* in the Galactic Center. We discuss the crucial role of S-stars in testing General Relativity (GR) in the strong gravity regime. Section 5 fully reviews HVS studies, including their search methods, the open catalog of hypervelocity stars, and the discussion of observational confirmation of central ejection, which is a distinctive feature of the Hills mechanism [13]. In that section, we also present the program of the search for HVSs by the Gaia space telescope (Global Astrometric Interferometer for Astrophysics). Section 6 discusses the prospects of searches for stars with relativistic velocities by forthcoming space missions that can address a modern astrometry challenge — the analysis of photometric and spectroscopic detection thresholds of faint objects at intergalactic distances. In conclusion (Section 7), we discuss the prospects for new knowledge from studying stars with relativistic velocities, new physics, and the improvement of fundamental laws of gravitation.

2. Stars with anomalous kinematics

From ancient Greek science (5th–6th centuries BC), the paradigm of immobile stars prevailed in astronomy for almost two thousand years. Over this time, the background of immobile stars played the role of a convenient reference frame to study periodic phenomena related to the motion and phases of the Moon, daily and annual changes in the Sun's location in the sky, as well as the visible motion of the five planets known at that time. The explanation for this fact, possibly, is not related to the low sensitivity of astronomical instruments in the pre-telescopic era: it took more than a century after the invention of the telescope by Galileo Galilei in 1609 before the paradigm changed. In addition, it is known how highly accurate measurements by eastern medieval astronomers were — 15 arcminutes (Ulugh Begh, the first half of the 15th century) and during the flourishing of European science — around one arcminute (Tycho Brage, the end of the 16th century). Perhaps the unshakable authority of the Hipparcos catalog and 'The greatest treatise' of Ptolemy was responsible for that. Needless to say, even the revolutionary theory by Copernicus preserved the concept of *sphaera stellarum fixarum*.

The Hipparcos catalog added by Ptolemy remained over all this time the indisputable 'top' of positional astrometry. Each subsequent generation of astronomers matched the results of their measurements with data on more than 1,000 stars from the famous catalog to improve the precession constant. This tradition was abandoned in 1718 by Edmond Halley, the royal astronomer of Greenwich Observatory, who noticed a difference in the position of the three brightest stars in the northern hemisphere: Arcturus, Surius, and Aldebaran, compared to the Hipparcos–Ptolemy catalog, and made an inference about the proper motion of stars. This discovery offered a qualitatively new approach for studies of the Galactic structure, encouraged the construction of the first kinematic models, including the determination of the solar motion apex, and accelerated the solution to the long-standing problem of determining annual stellar parallaxes.

2.1 'Flying' and 'runaway' stars: early observations and interpretations

As long as visual methods were applied in astrometry, the proper motions and coordinates could be measured only for the brightest and closest stars. By the end of the 18th century, when Maskelyne and Laland determined the proper motion of about two dozen stars, some of them were poetically dubbed 'flying' stars. Thus, the historically first class of stars with anomalous kinematics appeared. In the 19th century, this class included a whole 'pleiad' of candidate stars, including Lacaille 9352, the Piazzi star (61 Cyg), Groombridge 1830, the Kapteyn star, and in early 20th century the Barnard star. By 1920, the nature of these 'fast' or high-velocity stars (as they are called in the western scientific literature) was understood. They are stars of the late spectral class with masses of several tenths of the solar mass moving

with a space velocity of up to ~ 300 km s^{-1}, significantly higher than the peculiar velocity of near-solar stars ($\sim 20-30$ km s^{-1}).

Lindblad's idea [4] on the differential rotation of the Galaxy consisting of different mutually penetrating stellar subsystems rotating around a common center was well suited to explain these 'flying' stars populating the slowly rotating halo subsystem. By 'falling' from high orbits, these stars are accelerated to high velocities by the Galaxy's gravitational field during the galactic disk crossing. However, this is a visible effect of fast motion arising due to the different directions of motions of stars in the disk and halo.

By the 1960s, one more group of high-velocity stars at ~ 100–300 km s^{-1} moving opposite the 'flying' stars was found. They were young stars of the early ($B-A$) spectral class with masses of several solar ones, which were apparently 'escaping' from the disk into the halo. Following Walter Baade's suggestion [46], they were dubbed 'runaway' stars. Their anomalous kinematics were explained by Poveda's dynamical scenarios of the evolution of young stellar clusters and O–B associations [47], which are accompanied by violent collisional activity leading to stellar ejections from the cluster and disruption of multiple (at least triple) stellar systems.

The disruption of binary stars could also result in the accelerated motion of one of the components due to the explosion of another component as SN1b/c supernova. This scenario, suggested by Zwicky in 1957 [7], has a feature that high-resolution radio observations can probe. Namely, supersonically moving stars accelerated after the explosion of the second companion should form head bow shocks in the interstellar medium [8]. Both stars and pulsars, PSR 2224 + 65 (~ 1000 km s^{-1}) [9], for example, observationally supported the kinematic anomaly.

Presently, based on Hipparcos observations, a catalog of 'runaway' stars within three kpc from the Sun is being created. In addition, there is a photo-catalog of 'runaway' stars with head bow shocks detected in the infrared (IR) range by the WISE (Wide-field Infrared SUrvey Explorer) mission [8]. The propagation of interstellar shocks in a homogeneous molecular medium with a magnetic field is investigated using 3D hydrodynamic models. The shock form is studied depending on the magnetic field orientation and homogeneity, velocity, and laminarity of the stellar wind and the parameters of the interstellar medium. Monte Carlo radiation transfer calculations enabled bow shocks radiating in the IR and radio bands to be simulated and their geometry with actually observed fronts of runaway stars to be compared, providing prospects to probe the physical conditions and features of the ejection.

Presently, about 100 escaping stars are known, which is acceptable for the statistical analysis which, in particular, was carried out by Napiwotzky and Silva [48] by reconstructing the ejection trajectories of the 'escaping' stars. The reconstruction was performed by back-integrating in time the equations of motion of the stars using their current positions and velocities. This enabled the determination of the ejection place, the initial ejection velocity, and the star's mass at the moment of ejection. The obtained results were plotted on an 'initial velocity ejection — star mass' diagram that identified ten stars with a high initial ejection velocity (350–500 km s^{-1}) exceeding the Galactic second cosmic velocity at the ejection place. Thus, the statistical method uncovered a new class of stars with anomalous kinematics, dubbed 'hyper-runaway' stars. This name reflects, first, the fact that they are unbound from the Galaxy, and, second, the relation to the 'runaway' stars, because the ejection occurred in the upper disk layers in all cases. The first object of this class a B-type supergiant, HD 271791, was discovered in 2008 by Heber [49]. To date, nine stars 'hyper-runaway' from the disk and no longer bound to the Galaxy have been discovered [36].

2.2 Prediction of hypervelocity stars. Hills scenario in the classical three-body problem

As early as the beginning of the 1970s, Lynden-Bell and Rees suggested that both active galaxies and 'silent' centers of other galaxies like the Milky Way can harbor SMBHs [50]. Somewhat later, the idea of indirect searches for the massive central body appeared: in 1988, Jack Hills proposed the dynamical scenario of capture of a binary star (BS) by a nonclassical object such as a black hole [13]. Hills's calculations were performed in the framework of Newtonian mechanics. For a statistical ensemble of 250 initial configurations, the transition of a BS with component masses ($1M_\odot; 1M_\odot$) and the major semiaxis (in the range of 0.01–0.1 a.u.) near an SMBH with a mass of $10^4-10^7 M_\odot$ was simulated. The initial configuration assumed an arbitrary orbital phase of the binary components and binary inclination to the SMBH when passing at 1–10 a.u. The numerical modeling suggested that one of the binary components can be ejected with a maximal velocity of ~ 4000 km s^{-1}.

Assuming a stellar density inside 0.25 pc around the Galactic Center of $10^7 M_\odot$ pc^{-3} and a velocity dispersion of 80–250 km s^{-1}, Hills estimated the birthrate of model hypervelocity stars at 10^{-4}–10^{-5} per year. Taking into account the mean ejection velocity of such stars (~ 1000 km s^{-1}), it is possible to evaluate that the characteristic time for an HVS to escape from the Galaxy is a hundred million years. This means that the number of such stars in the Galaxy is about several thousand. This is an approximate estimate because the model ignores the survival probability of the star during the ejection and galactic radius crossing, and, mainly, the capture probability at distances appropriate for HVS formation.

In this way, a new class of stars with anomalous kinematics was predicted, which, like 'hyper-runaway' stars, had a positive binding energy with the Galaxy but higher ejection velocity in the direction away from the Galactic Center. The presence of an SMBH offers a new acceleration mechanism of stars up to velocities that would earlier have been considered measurement errors. There are other HVS formation mechanisms.

2.3 Alternative scenarios for the generation of hypervelocity stars

The acceleration of one binary component due to the supernova explosion of the other limits the maximum possible velocity of the star by the parabolic velocity from the surface of the surviving component. This restriction, for example, for a $3M_\odot$ star (spectral class B) with a radius of $2.3\,R_\odot$ is about 700 km s^{-1}. Even higher velocities (up to 1600 km s^{-1}) can be obtained from the disruption of extremely close binaries containing helium stars of 4–10 $M_\odot$ and neutron stars. Presently, there is observational evidence of such rapid stars; for example, the pulsar PSR 2224 + 65 was ejected with a velocity of ~ 1000 km s^{-1} [9], and the binary white dwarf LP400-22 acquired a space velocity exceeding 800 km s^{-1} [51].

Approximately the same velocity limit is obtained in the dynamical scenarios considering collisions or close encounters of two BSs or a single and a binary star. In dynamic scenarios involving a black hole, the kinetic energy of ejections can be higher by one order of magnitude. According to formula (3) from paper [52],

$$v_{\rm eject} = \alpha\sqrt{\frac{GM}{A_{\rm min}}} \approx 275\,\sqrt[3]{\frac{M}{m}}\,\sqrt{\frac{m}{R}}, \qquad (1)$$

the maximum ejection velocity of a main-sequence star (1–3 $M_\odot$) from the vicinity of an SMBH with a mass of $10^6 M_\odot$ can exceed 20,000 km s^{-1}. Here, α is a coefficient of the order of one, M and m are the SMBH and stellar mass, respectively, and R is the stellar radius corresponding to the inner Roche lobe size $r_{\rm cri}$. For a star in a pair with such a nonclassical object as an SMBH, the survival condition is compulsory: the minimum possible large semiaxis $A_{\rm min}$ of the star–SMBH system should not be smaller than the tidal radius. Equivalently, the stellar component should remain inside its Roche lobe $R = r_{\rm cri} \sim 0.4 A_{\rm min}\sqrt[3]{m/M}$; otherwise, the star will be tidally disrupted.

One could expect higher accelerations around more massive SMBHs. However, with increasing SMBH mass, its proper size (the Schwarzschild radius) $r_{\rm sch} = 2GM/c^2$ also increases. For an SMBH with a mass exceeding $10^8 M_\odot$, the Schwarzschild radius is higher than the tidal radius $r_{\rm t} = 2^{4/3} R\sqrt[3]{M/m}$, marking the distance of a safe encounter of a star with the SMBH. The last bound orbit around an SMBH lies at two Schwarzschild radii [53]. The equality $2r_{\rm sch} = A_{\rm min}$ yields the limiting SMBH mass for a given star mass $M_{\rm cri} = c^3[(R/G)^3]^{1/2}[(32m)^{-1}]^{1/2}$. However, the energy of this orbit does not depend anymore on the SMBH mass, $U_{2r_{\rm sch}} = GMm/(2r_{\rm sch}) = 1/4mc^2$. Therefore, an SMBH with mass M exceeding $M_{\rm cri}$ will not produce higher velocity ejections. The limiting energy in the Hills ejection mechanism means the limiting ejection velocity of stars.

To assess the maximum possible ejection velocity, one should calculate the maximum possible momentum exchange between BS components when passing the orbital pericenter around the SMBH. Consider the mean motion of a BS in the central field of a much more massive third body (SMBH). This enables us to reduce the three-body problem to a two-body problem. By assuming the maximum momentum exchange when the BS components (with equal masses and radii, for simplicity) approach by the sum of their radii, $2R$, after which each of the binary components changes its motion to the opposite, $v \to -v$, the velocity change is $2v$.Thus, the maximum momentum exchange is $2mv$. As the exchange occurs at the pericenter, the resulting velocity is $v_{\rm p}+2v$, where $v_{\rm p}$ is the velocity in the pericenter. The energy gain at the pericenter, $\Delta E = m(v_{\rm p}+2v)^2/2 - mv_{\rm p}^2/2$, can be translated into the ejection velocity, $\sqrt{(2\Delta E/m)}$. By assuming a pericenter velocity of the order of the parabolic one and estimating the orbital velocity of the components from energy-momentum conservation, it is possible to find the limiting ejection velocities of stars with different masses in the field of an SMBH with different masses. For example, for a main-sequence star of the B spectral type with a mass of $3M_\odot$ and radius of $2.3R_\odot$, the maximum ejection velocity by an SMBH with a mass of $10^6 M_\odot$ is estimated to be about 8000 km s^{-1}.

The maximum ejection velocity from an SMBH with a critical mass of $10^8 M_\odot$ for a $3M_\odot$ star can be as high as $\sim$ 17,500 km s^{-1}. Similar velocities are obtained for a $1M_\odot$ star. Theoretical estimates show that stars' maximum possible ejection velocity by the classical Hills mechanism of the dynamical capture of a BS by the SMBH gravitational field is no higher than $0.1c$ [26].

2.4 Modified Hills scenario. Prediction of stars with relativistic velocities

Ejection velocities like those in the classical Hills mechanism can be obtained in other scenarios, for example, by the 'kick'-scattering of stars by a cluster of black holes [28], *in-spiralling* of a $(10^3-10^4)M_\odot$ black hole towards the Galactic Center [29], as well as by the capture of a star by a binary SMBH [54]. The possibility of binary and multipole black hole formation in galactic centers directly follows from the hierarchical galaxy formation model. According to formulas (6) and (7) from review [52],

$$\tau_{\rm GWR} = 10^8\left(\frac{A}{R_\odot}\right)^4\left(\frac{M}{M_\odot}\right)^{-3}\ {\rm yr}, \qquad (2)$$

$$v_{\rm GWR} = 310\left(\frac{M}{M_\odot}\right)^{1/8}\left(\frac{\tau_{\rm GWR}}{10^8}\right)^{-1/8}\ {\rm km\ s^{-1}}, \qquad (3)$$

for a binary SMBH with $10^6 M_\odot$ components and a major semiaxis of one a.u. ($\approx 50r_{\rm sch}$), for which the coalescence time due to gravitational wave emission $\tau_{\rm GWR}$ is $\sim$ 80 days, the ejection velocity can reach $0.1c$. For closer binary SMBHs with a large semiaxis of $\approx 5r_{\rm sch}$, the coalescence time shortens to 10 minutes, and the ejection velocity can attain $(1/4)c$. Further shrinking of the binary SMBH orbit shortens the coalescence time even more, reducing the probability of accidental capture of a star at this stage to zero.

The idea to include a second (host) SMBH instead of one of the BS components in the Hills scenario was proposed by Guillochon and Loeb, who calculated this mechanism in the three-body problem framework [41]. Their modeling showed that the limiting ejection velocity in the modified Hills mechanism could attain $(1/3)c$. This result was obtained from the velocity distribution derived from more than 10^5 independent numerical simulations of scattering of a binary system consisting of the host SMBH with mass M_2 and the ordinary star with mass M_3, passing near the more massive SMBH with mass M_1. About 1% of the calculations with circular binary orbits showed the maximum ejection velocity. In these cases, the flight to the central SMBH occurred in a parabolic orbit with an eccentricity of ~ 1 and a pericenter distance of ten radii of the last stable orbit ($20r^1_{\rm sch}$). The gravitational field of both SMBHs is homogeneous. Thus, a new class of stars with anomalous kinematics, 'semi-relativistic stars', was announced.

Guillochon's and Loeb's [41] use of empirical relations derived from Sari's numerical calculations [55] and the admission of the binary orbit decrease to three-four Schwarzschild radii of the second SMBH raised a question about star survival during the ejection. It was necessary to repeat the simulations in an approach of the modified Hills scenario in the N-body problem framework describing the stellar structure as gravitationally bound elements. Section 3 will present the methods and the calculation results demonstrating a higher ejection velocity of up to $c/2$ [42]. The dynamics of the star disruption enabled correcting conditions of star survival and improving upon the fraction of 'successful' events that proved to be one order of magnitude smaller than predicted in [41].

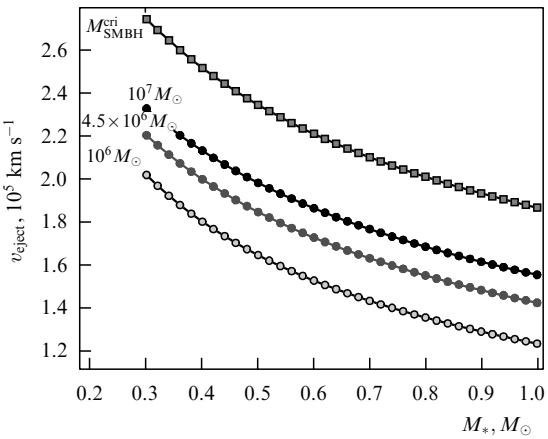

Figure 1. Velocity of a star as a function of its mass ejected from a binary system with an SMBH ($4.5\times10^5 M_\odot$) passing near the central SMBH (masses are shown in the figure) [42].

Theoretical estimates of the maximum possible ejection velocity in the modified Hills scenario allow even higher velocities, $(2/3)c$, which can be obtained by taking into account the full momentum exchange between the binary components, resulting in a velocity increase of $2v$ at the pericenter. As one of the binary components is an SMBH, the orbital velocity of the binary system is

$$v=\sqrt{\frac{2GM_2}{r_{\rm t,2}}},$$

where $r_{\rm t,2}$ is the tidal radius of the host SMBH. Then, the energy increase at the pericenter, considering the relativistic velocity addition law, is

$$\Delta E=mc^2\left(1-\frac{\tilde v^2}{c^2}\right)^{-1/2}-mc^2\left(1-\frac{v_{\rm p}^2}{c^2}\right)^{-1/2},$$

where $\tilde v=(v_{\rm p}+2v)/(1+2v\,v_{\rm p}/c^2)$ can be transformed into the ejection energy. The ejection velocity is

$$v_{\rm eject}=c\sqrt{1-\frac{M_3^2c^4}{\Delta E^2}}.$$

Figure 1 shows the ejection velocity of the star as a function of its mass in the modified Hills scenario [42]. The estimates are obtained for stars with masses of $(0.3-1)M_\odot$ paired with an SMBH with a mass of $4.5\times10^5 M_\odot$ at the pericenter of the central SMBH with a mass ranging from $10^6 M_\odot$ to the critical value $M_{\rm cri}$, depending on the star mass. Thus, the relativistic dynamics in the modified Hills scenario can explain the origin of anomalous stellar velocity compared to the speed of light.

2.5 Classification of stars with anomalous kinematics

The above data show that the modern kinematic hierarchy of stars with anomalously high space velocities includes five classes:

(1) 'flying stars' ($\leqslant 300$ km s^{-1});
(2) 'runaway stars' ($\leqslant 300$ km s^{-1});
(3) 'hyper-runaway stars' ($\geqslant 400$ km s^{-1});
(4) 'hypervelocity stars' ($\geqslant 700$ km s^{-1});
(5) 'stars with relativistic velocities' ($\geqslant (1/3)c$).

Here, the notion of class is rather conditional because of the phenomenological separation of objects. Interestingly, unlike the third and fourth classes, stars in the first two classes were first discovered and only after that interpreted. As mentioned in Section 2.1, the 'rapidly escaping' stars were first singled out on the reconstructed 'star ejection velocity — mass' statistical diagram, and, one year later, Heber obtained the first observational confirmation of such stars: HD271791, a class *B* supergiant with the spatial velocity exceeding the escape velocity at the ejection point [49].

The first hypervelocity star was discovered by Brown et al. in 2005 at a heliocentric distance of ~ 70 kpc [15], although such stars were predicted by Hills already in 1988 [13]. By now, several dozen such stars are known. However, class five stars with relativistic velocities have not been discovered — they are hypothetical objects so far.

Note the predictive capabilities of numerical simulations that played an essential role in the discovery of new classes of kinematic anomaly. We consider them in the next section.

3. Numerical modeling of Hills scenario

The exploration of rare objects like HVSs is based on the probabilistic approach enabling one to find intervals of the rare events and their correlations. This standard approach in the epoch of supercomputers investigates a large statistical ensemble of initial states to fetch 'successful' events, HVSs in our case. The method has two modeling stages: first, in the three-body problem, and then, in the *N*-body problem formulation.

The initial state is a spatial configuration of three bodies, including the internal orbit of a BS with arbitrary component phases and a major semiaxis and the external randomly oriented orbit of BS motion around a central SMBH. The external orbit is elliptical with an apocenter distance of $10^5 R_\odot$ to imitate BS approach to SMBHs from 'infinity'.

An initial set of 10^4 proper BS orbits were randomly generated for a fixed pericenter distance of the external orbit around a central SMBH with a mass of $3.4\times10^6 M_\odot$. The well-studied close binary MR Cyg was used as the prototype in all variants. This binary has the component masses $m_1=4.5M_\odot$ and $m_2=2.5M_\odot$ with radii $R_1=4.07R_\odot$ and $R_2=3.17R_\odot$, large semiaxis $A=11.3R_\odot$, and orbital velocities 122.68 km s^{-1} and 220.83 km s^{-1}, respectively.

BSs with a wide range of large semiaxes were modeled: from close binaries with separations comparable to the star sizes to wide systems [55]. Five initial values of A were considered: $11.3R_\odot$, $56R_\odot$, $125R_\odot$, $282R_\odot$, and $425R_\odot$. Pericenter distances varied in the range bounded by the BS tidal radius estimated from the balance of tidal forces $F_{\rm t}=GM(m_1/r_{\rm t}^2-m_2/(r_{\rm t}+A)^2)$ and the BS self-gravity $F_{\rm s\text{-}g}=Gm_1m_2/A^2$ from above and by the tidal radius of each component from below. For example, for a star with a mass of $4.5M_\odot$ and radius of $4R_\odot$ captured by an SMBH with a mass of $10^6 M_\odot$, the tidal radius $r_{\rm t}$ is $310R_\odot$; by crossing it, the star will be tidally disrupted. As a result, BS orbits with $r_{\rm p}\in[r_{\rm t}-150r_{\rm t}]$ were considered. The whole statistical ensemble of the initial three-body systems with arbitrary orbital phases of the components and binary inclinations comprised 1,240,000 configurations.

3.1 Analysis of the velocity spectrum in the classical Hills scenario. Three-body problem

The search for HVSs in model calculations is based on the analysis of the total energy of each binary component over one orbital revolution around the SMBH. It is reduced to

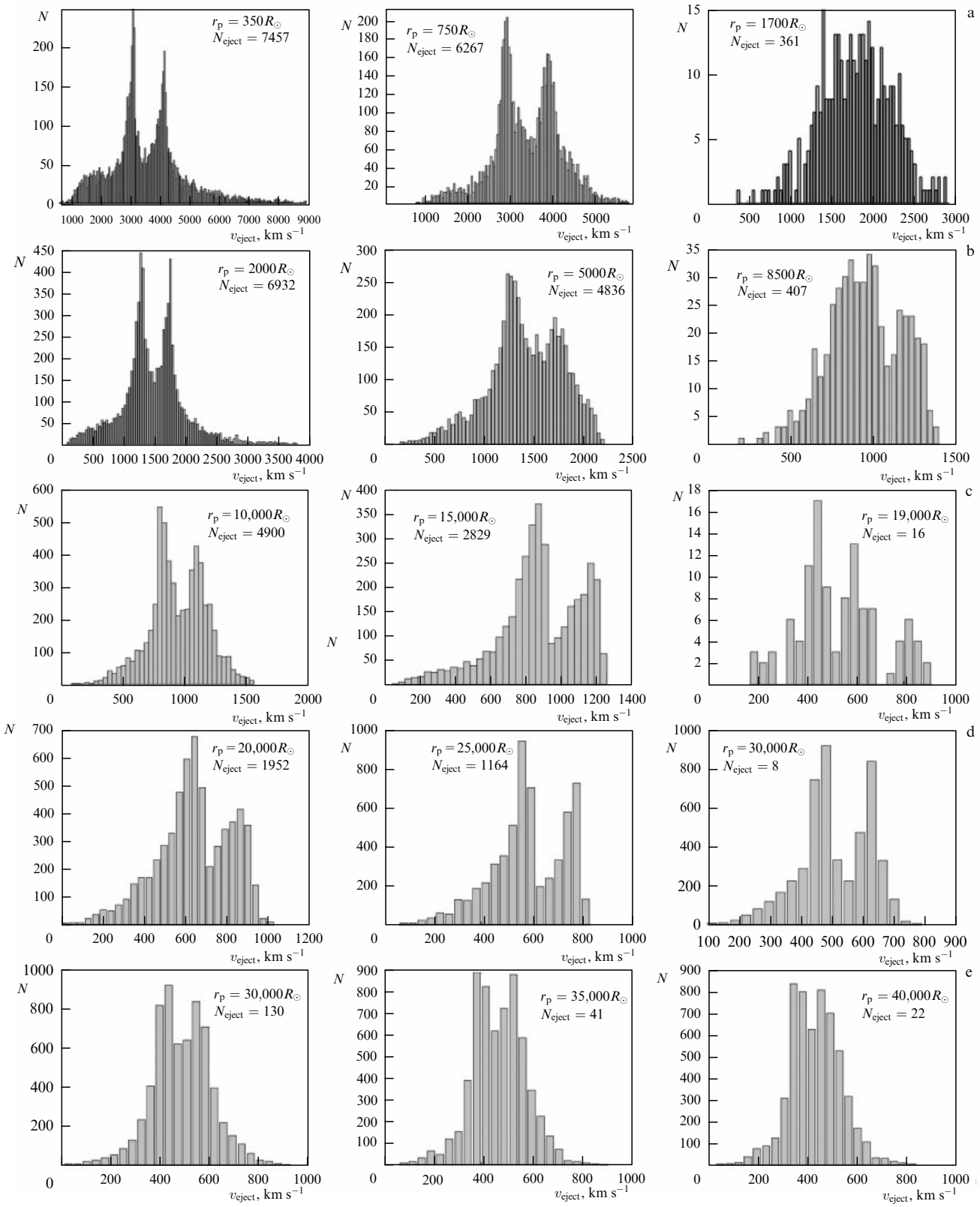

Figure 2. Velocity distributions of ejected BS component as obtained from numerical modeling of Hills scenario in the three-body problem formulation [55]. Calculations for a BS ($4.5M_\odot + 2.5M_\odot$) passing by an SMBH with mass $3.4 \times 10^6 M_\odot$ for three arbitrary r_p (three plots in a row). Each row corresponds to five BS major semiaxes: (a) $11.3R_\odot$, (b) $56R_\odot$, (c) $125R_\odot$, (d) $282R_\odot$, (e) $425R_\odot$. Inserts show values of r_p and number of HVSs N_{eject}.

integrating Newtonian equations of three-body motion in the velocity formulation of the Verlet and Weis algorithm [56]. The ejected object is the BS component with total positive energy after one orbital revolution. The kinetic energy of the ejection will be determined by the total energy increase ΔE provided that the ejected component will go to infinity with zero potential energy. This simple assumption enables estimating the ejection velocity $v_{eject} = \alpha' \sqrt{2\Delta E/m}$, where

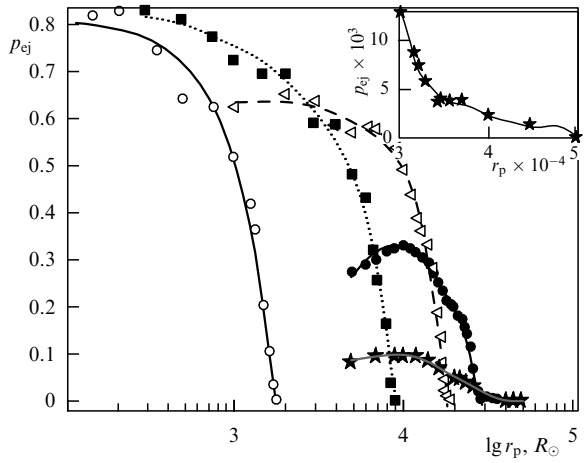

Figure 3. Probability of BS ejection from a binary system ($4.5M_\odot + 2.5M_\odot$) as a function of r_p for an SMBH with mass $3.4 \times 10^6 M_\odot$. Curves are calculated for five values of the BS major semiaxis. From left to right: $11.3R_\odot$ (circles), $56.5R_\odot$ (dark squares), $125R_\odot$ (triangles), $282R_\odot$ (dark dots), $425R_\odot$ (dark stars). The insert zooms the large-scale tail for the variant with the major semiaxis $425R_\odot$ [55].

α' is the coefficient of the order of one. This information yields the velocity spectrum characterizing the dynamics of the statistical ensemble from 10^4 orbital trials calculated for fixed r_p and A (Fig. 2).

The HVS candidates (N_{eject}) with $v_{eject} > 750$ km s^{-1}, according to the criterion by Wu et al. [27], are selected from the velocity distribution, yielding the ejection probability as the ratio of 'successful' events to the total number of trials, $p_{ej} = N_{eject}/10^4$. Figure 3 shows the ejection probability p_{ej} as a function of r_p for all semimajor axes of BSs. Unlike close binaries giving 'guaranteed' stellar ejection ($p_{ej} \sim 0.6-0.8$) from the SMBH vicinity at small $r_p \leqslant 4r_t$, wide binaries were first ignored due to a high disruption probability before they reached the tidal radius. However, numerical simulations of binary star scatterings on SMBHs showed that wide binaries ($A \to 500R_\odot$) significantly increase the HVS ejection 'corridor'. Thus, HVS formation can effectively occur within ~ 1 mpc, depending on the BS major semiaxis, and the HVS, p_{ej} ejection probability decreases by orders of magnitude ($< 10^{-3}$).

In order to describe realistic ejection from the SMBH vicinity due to binary star capture, a much larger number of factors should be taken into account. However, even at this description level, it is clear that probability p_{ej} is only one component of the HVS formation probability in the Galaxy. At least three additional factors should be considered: the BS capture probability into the potential HVS generation zone p_c, the survival probability of the ejected star p_s, and the probability of preserving the hypervelocity over the entire galactic scale p_g. To assess the third factor, the energy losses of an HVS moving in the regular field of the Galaxy are derived from the calculated velocity spectra. The model Galactic potential includes the contributions from the disk, bulge, halo, and dark matter [57]. The modeling of 'free paths' of the ejected stars in the collisionless Galactic potential suggested a high value of p_g guaranteeing HVS status up to the Galactic outskirts at 200 kpc [55].

The point-like representation of the stellar components enables predicting their survivability during close fly-bys near SMBHs using its tidal radius calculated from the theory of gravitation. A more rigorous estimate of the survival probability of a star ejected from the SMBH vicinity required calculations in the N-body problem frame, where N is the number of structural elements of the star.

3.2 Survival criteria of stars ejected from the SMBH vicinity. *N*-body problem

The N-body modeling was first applied in physics to study and predict properties of matter consisting of atoms interacting according to a specific law. The numerical modeling of interacting N atoms was dubbed *the method of molecular dynamics*, which enables investigating a wide range of physical problems.

By analogy with matter or the Galaxy, where it is possible to trace the motion of separate atoms or stars, a star could be represented by a collection of N individual structural elements. In this case, we could 'watch' the change in the stellar state under the action of tidal forces and estimate the limiting flyby distance where the star may still avoid fatal destruction in the SMBH gravitational field.

Calculations in the N-body formulation preserve the probabilistic approach, involving a random statistical ensemble of the initial orbital configurations of the star in the SMBH field with an arbitrary orbital inclination and pericenter distance. The SMBH is considered a point-like source, while the star is a finite-size object comprising N identical structural gravitationally interacting elements. The elements are taken as spheres with a fixed radius and an initial polytropic and homogeneous radial density distribution. The gas pressure is imitated as a prohibition on elements approaching due to gravitational interaction. The star can change its form and be destroyed by keeping the total volume of the fragments [26].

The star's motion in the SMBH central field is the motion of N structural elements written in the Newtonian form. The equations of motion are integrated using the velocity formulation of the Verlet and Weis algorithm [56], conserving the total energy, momentum, and angular momentum. In the Cartesian coordinates, the equations of motion have a simple form:

$$M_k \frac{\mathrm{d}^2 x_\alpha^k}{\mathrm{d}t^2} = -\frac{\partial U}{\partial x_\alpha^k}, \qquad k = 1, \ldots, N, \qquad \alpha = 1, 2, 3, \quad (4)$$

where $U = -1/2 \sum_{i=1}^{N} \sum_{j=1_{i \neq j}}^{N} GM_i M_j / \mathbf{r}_{ij}$ is the gravitational interaction energy of the star's elements.

This simple (call it 'gravitational') stellar model is computationally cheap and enabled us to effectively carry out a statistical suite of simulations to find the key stellar parameters, including its mass loss and the impact parameter $\beta = r_t/r_p$ characterizing the penetration of the star 'under the barrier' of the tidal radius r_t. Figure 4 illustrates the dynamics of tidal deformations of a star captured by the SMBH field ($10^6 M_\odot$) for different flybys [26].

The numerical results suggest that, in the polytropic model with index $n = 3$, the star plunges much deeper 'under the tidal radius barrier' ($\beta = 3.5$), and the mass-loss can attain $\sim 80\%$. In contrast, in the homogeneous ball model, already $\sim 10\%$ mass-loss destroys the star, although its plunging 'under the tidal radius barrier' corresponds to $\beta \sim 1.38$. Importantly, only part of the envelope is lost during the short-time Roche-lobe overfilling by the star's rarefied extended outer envelope, and the star itself is preserved.

The obtained criteria were checked by modeling tidal destructions of stars in the SMBH field with hydrodynamical

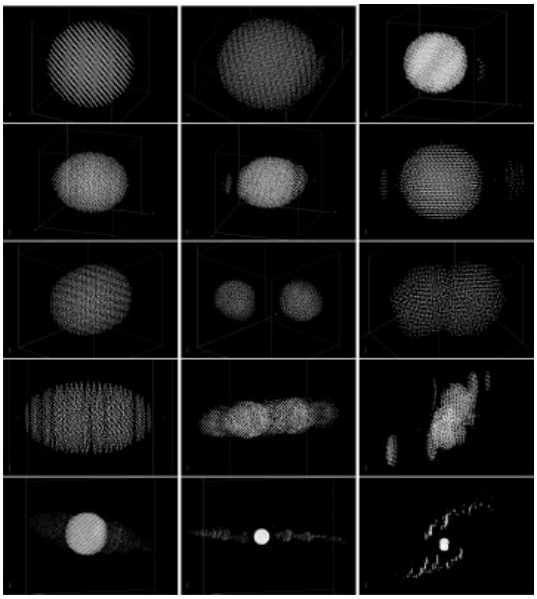

Figure 4. Model calculations in the N-body formulation ($N = 3600$) of the dynamical evolution of a binary star ($4.5M_\odot$, $4R_\odot$) during pericenter passage around an SMBH ($10^6 M_\odot$) [26]. First four rows are for the homogeneous ball model tested for orbits with r_p: (a) $275R_\odot$, (b) $250R_\odot$, (c) $220R_\odot$, (d) $200R_\odot$. Fifth row (e) corresponds to a polytropic star ($n = 3$) in orbit with $r_p = 140R_\odot$. Evolution proceeds from left to right. Tidal radius in this problem is $r_t = 310R_\odot$.

3D codes using Euler-Lagrange grid methods and comparing them with analytical calculations based on the affine formalism [58]. Such calculations were initiated already at the beginning of the 1980s by the problem of the nature of the brightest outbursts ubiquitously observed in galactic nuclei. Starting from papers by Lynden-Bell [59] and Dokuchaev and Ozernoy [60], these outbursts are related to the possible tidal disruptions of stars by SMBHs, which occasionally (due to the nonstationary accretion) 'reanimate' an SMBH by turning it into a quasar. However, there are other reasons for SMBH rebrightenings, whose contributions could be improved by statistics on tidal disruptions of stars, but which remain quite uncertain thus far [61, 62].

A comparison of the simple 'gravitational' model of a star [26] with more realistic models of the stellar internal structure (for example, the model of embedded ellipses by Ivanov and Novikov [63] or the hydrodynamic model by Guillochon and Ramirez-Ruiz [64]) showed that the output parameters of the homogeneous ball presented in the 'impact parameter — stellar mass-loss' diagram fall on the region of the middle model values [63, 64] calculated for $n = 3$ and $n = 3/2$ polytropes (Fig. 5).

To estimate the survival probability of a star ejected as an HVS, we used a statistical ensemble of 350 initial configurations of the binary star MR Cyg with an arbitrary orbital phase of the components, binary orbital inclination, and pericenter distance $r_p \in [(1/3)\, r_t - 4r_t]$ [65]. The orbital motion of the binary components and their mutual gravitational interaction corrected the star's survival criteria [55, 65]. In the N-body modeling, three final states of the close binary system after its approach to the SMBH have been distinguished: the destruction of the star, the coalescence of the components into a single star, and the separation of the components into two unbound orbits, the outer of which is identified with the HVS candidate (Fig. 6).

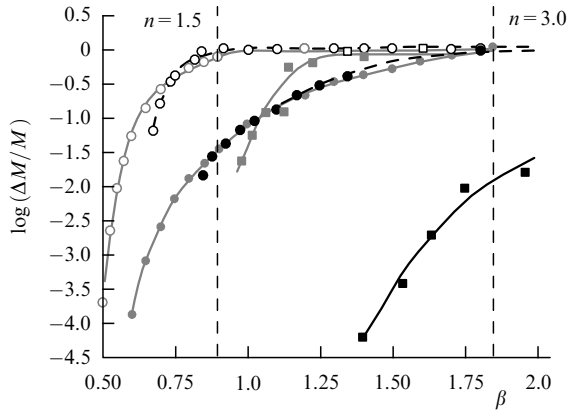

Figure 5. Mass loss of a star (initial mass $1M_\odot$) $\Delta M/M$ due to tidal disruption in the SMBH field ($10^6 M_\odot$) as a function of impact parameter β. Dots and circles are for an $n = 3$ and $n = 3/2$ polytrope. Grey and black dots show the results [64] and [63], respectively. The filled squares present the results [26] for a homogeneous ball (grey) and a polytropic ball with index $n = 3$ (black). Dashed lines show total disruption limits for polytropic stars with $n = 3$ and $n = 3/2$ obtained in [63, 64].

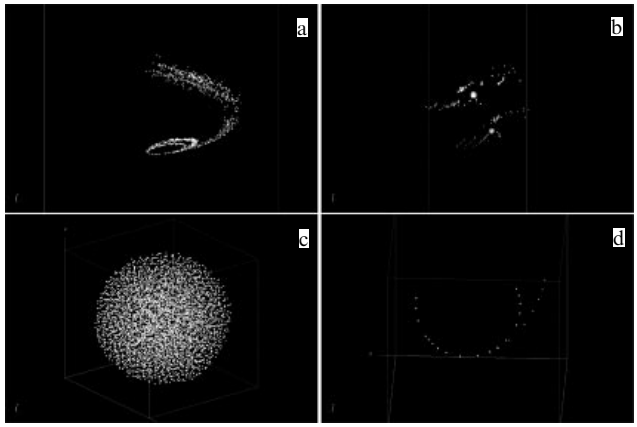

Figure 6. Modeling of dynamical evolution in the N-body formulation ($N = 5300$) of the components of MR Cyg ($4.5M_\odot$, $4R_\odot$; $2.5M_\odot$, $3.2R_\odot$) during pericenter passage around an SMBH ($10^6 M_\odot$) [65]. BS components are approximated as polytropic balls ($n = 3$) and computed for orbits with $r_p = 85R_\odot$, $150R_\odot$, $300R_\odot$, $500R_\odot$ (plots a, b, c, d, respectively). Shown are examples of possible consequences of the pericenter passage: destruction of the components (a), ejection of the primary component of MR Cyg as an HVS ($v_{\rm eject} = 2760$ km s^{-1}) with a 15% mass-loss (b), coalescence of the components (c), and tangential ejection to the pericenter arc of the secondary component of MR Cyg as an HVS ($v_{\rm eject} = 2300$ km s^{-1}) without mass-loss (d).

Calculations involving more massive SMBHs ($\geqslant 10^6 M_\odot$) revealed the dependence of the mass-loss rate and the maximal ejection velocity on the pericenter approach and the SMBH mass (Figs 7, 8) [26]. For the polytropic model, the mass loss has not exceeded 25% of the initial mass, and the dispersion of structural fragments has not exceeded double the initial stellar radius. Thus, the calculations yielded the criterion (the 25% mass-loss level) of the structural entity conservation of a star approaching an SMBH, which was two-three times smaller than the theoretically admissible tidal radius estimate.

The statistics on the final states yielded the survival probability estimate of a $4.5M_\odot$ star ejected as an HVS from the SMBH ($10^6 M_\odot$) vicinity in the Hills scenario (Fig. 9). According to computations [26, 65] carried out in the three-body and N-body setups, the survival probability of the star

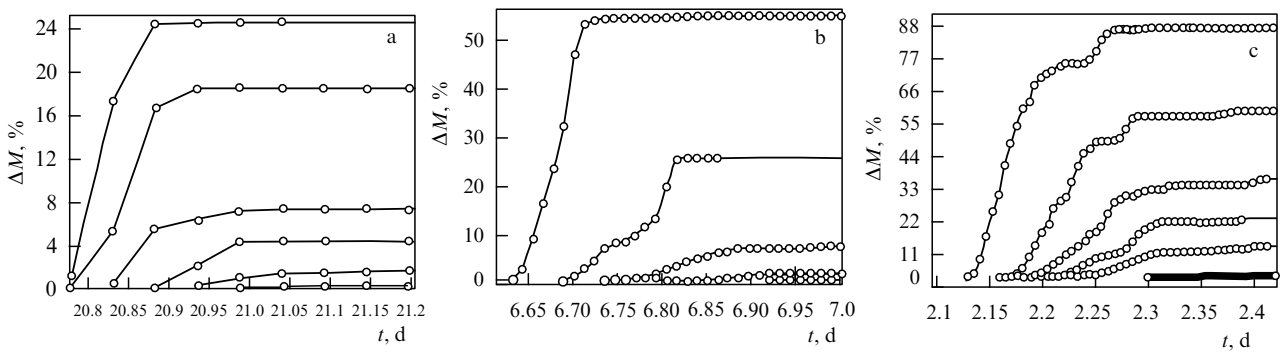

Figure 7. Mass-loss ΔM as a function of time t for a single star ($4.5M_\odot$, $4R_\odot$) passing a fixed pericenter distance r_p [26]. Star is approximated as a polytropic ($n = 3$) ball in the N-body problem formulation ($N = 3500$). Presented are calculations for three SMBH masses: $10^6 M_\odot$, $10^7 M_\odot$, $10^8 M_\odot$ (plots a, b, c, respectively). Curves from top to bottom correspond to orbits with $r_p = 85R_\odot$; $90R_\odot$; $100R_\odot$; $115R_\odot$; $125R_\odot$; $150R_\odot$ (a), $r_p = 150R_\odot$; $200R_\odot$; $250R_\odot$; $300R_\odot$; $400R_\odot$ (b), $r_p = 250R_\odot$; $350R_\odot$; $400R_\odot$; $450R_\odot$; $500R_\odot$; $750R_\odot$(c).

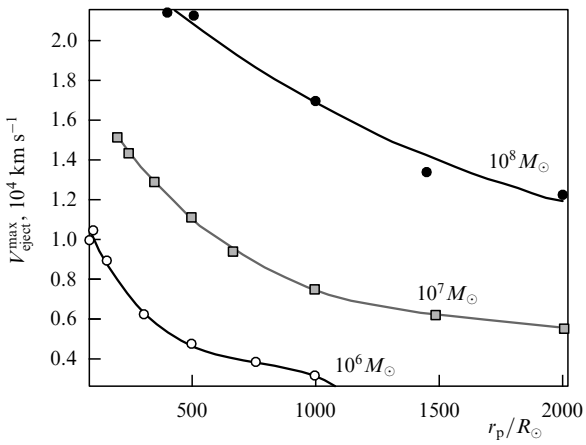

Figure 8. Dependence of maximum ejection velocity $V_{\rm eject}^{\rm max}$ of one of the BS components on r_p. Curves are obtained from velocity distributions calculated in the three-body problem formulation for SMBHs with masses $10^6 M_\odot$, $10^7 M_\odot$, $10^8 M_\odot$ (from top to bottom) [26].

vanishes for $r_p < 85R_\odot$, which is $(1/3)r_t$, and by approaching the SMBH at the distance $r_p \in [1/3r_t - r_t]$, the star can survive. At distances exceeding $3r_t$, the survival probability is unity, since no HVS ejections can occur there.

These results revealed an effect similar to the tunnelling effect in nuclear physics: an capability of the star to plunge 'under the tidal radius barrier' for a short time, avoiding tidal disruption and 'extracting' acceleration for the ejection as an HVS. The pericenter passage lasts for seconds, as opposed to a binary period of ~ 50 days in the model calculations.

Thus, the model results in the N-body problem formulation suggest that it is insufficient to rely only on the velocity distribution to probe the HVS status.

3.3. Dynamical model of capture of a binary star into the SMBH vicinity

According to recent observations, the stellar populations inside the central parsec number tens of thousand stars; at 0.1 pc from the center, their number decreases to several hundred, at 0.01 pc there are ~ 30 B-stars, and inside the central milliparsec (mpc) there is only one star [32–34]. Such low statistics suggest a random character of stellar captures in the central Galactic region. Therefore, to estimate the capture probability by the SMBH, we have chosen the model of layer population of the central Galaxy [66] consistent with the observed stellar density gradient.

The population model reflects the present-day diffusive SMBH growth stage when the SMBH has already been formed and changes its mass due to scattering (diffusion) of stars from nuclear clusters during their pericenter passages. This is a long-lasting process determined by the tidal braking of stars in the SMBH field $\tau_{\rm dif} \sim v^3/(\pi G^2 \rho_{\rm cl} M_{\rm SMBH})$, where v is the velocity dispersion of stars of the order of the

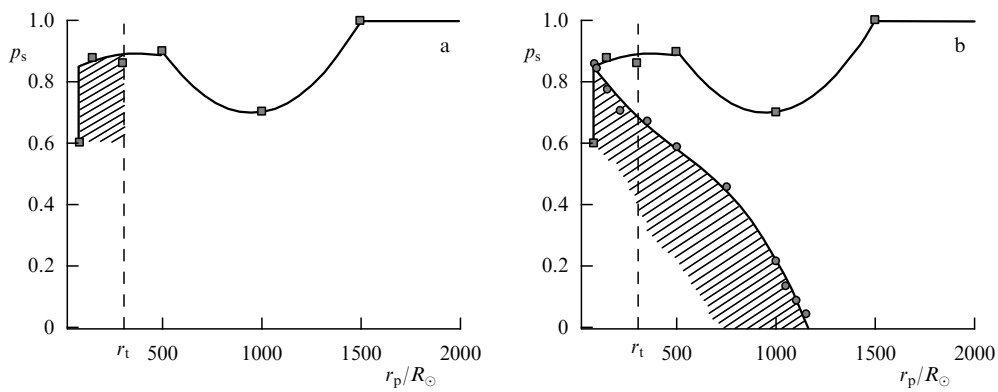

Figure 9. (a) Survival probability of a star ($4.5M_\odot$, $4.07R_\odot$) ejected by an SMBH ($10^6 M_\odot$) as a function of r_p. Model curve is obtained by calculating 300 arbitrary initial configurations in the N-body problem formulation for a polytrope with index $n = 3$ [26]. (b) Same as in (a) considering the ejection probability of one BS component with a velocity above 750 km s^{-1} as calculated from 200,000 initial configurations in the three-body problem formulation [26]. Hatching left-of-dashed line in both plots shows the tunnelling zone, in which the star can survive and can be accelerated up to $0.03c$.

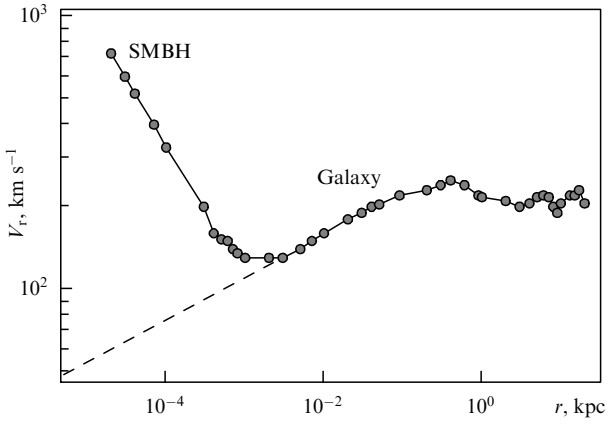

Figure 10. Logarithmic rotational curve of the Galaxy [67]. Curve is 'sewn' from two branches: the inner one ($r < 1$ pc), dominated by SMBH gravity, and the outer one ($r > 1$ pc), controlled by the Galactic potential. External branch is extrapolated into the inner region $r < 1$ pc (dashed curve) to estimate the central population.

Keplerian velocity, $\rho_{\rm cl}$ is the mean density of the central cluster, and $M_{\rm SMBH}$ is the SMBH mass.

Initially, the model cluster stars are in regular orbits confined to a spherical layer 0.01 pc $< r <$ 0.1 pc. After a series of random pair approaches, the stellar orbits get perturbed, leading to the 'fall' of some stars into the region < 1 mpc centered on the radio source Sgr A*. This is the limit justified by calculations of the region of potential HVS generation [55] by the Hills mechanism [13]. Therefore, another component that remained after the HVS ejection may be an S-star candidate.

The central population model [66] used the integral Galactic three-component (disk, bulge, halo) rotational curve calculated from high-resolution CO and HI spectroscopy and OH and SiO infrared star masers [67]. 'Sewn' from two branches, the external and internal, the rotational curve (Fig. 10) characterizes the SMBH influence sphere, which controls the star motion at $r < 1$ pc according to Kepler's law and demonstrates the effect of the Galactic potential on stars in orbits more than one pc away from the center. The external branch of the rotational curve reflects the real population of stars in all Galactic subsystems, which enables an extrapolated estimation of the dynamical mass clustered within 0.01 pc $< r <$ 0.1 pc to predict the central Galactic population without mass segregation (Fig. 10).

The mean time of 'expulsion' of a BS from the spherical layer into the $r < 1$ mpc region is estimated through the time between two subsequent orbital perturbations τ and the number of single perturbations n, i.e., $\bar{t} = \tau n$. By analogy with the theory of collisional processes, τ is equivalent to the free-path length λ for a given velocity dispersion $\sigma_{\rm V} \sim$ 60 km s^{-1} according to the circular rotational velocity [67]. Free-path length λ, in turn, is determined by the effective scattering radius $r_{\rm eff} = 2Gm/\sigma_{\rm V}^2$ that characterizes the distance between stars with mass m at which their gravitational interaction energy matches the kinetic energy.

Each perturbation changes the orbital pericenter, whose location is recalculated from the equation of motion by assuming that the BS remains bound in the central SMBH field. This approach significantly simplifies the analysis of perturbations, not requiring the direct calculation of the BS orbit. The capture event corresponds to the BS pericenter crossing the potential HVS generation region at a distance of one mpc from the SMBH.

The value inverse to the average 'expulsion' time is the BS capture probability into the potential HVS generation region $p_{\rm c}$. All possible initial BS locations in the spherical layer (0.01 pc $< r <$ 0.1 pc) from which the star can be expulsed yield a total capture probability of $p_{\rm c} \approx 2 \times 10^{-5}$ per year. Also, it is necessary to consider that, in numerical experiments [55], ejections of one of the BS components occurred at $r_{\rm p} < 1$ mpc, warranting the capture of the second BS component as an S-star with a probability of $p_{\rm c}(r_{\rm p}/1\ {\rm mpc})^3$.

Therefore, the HVS formation probability in the Hills scenario p is estimated as the joint probability of the occasional passage of a star near an SMBH at distances closer than one mpc, which would result in the simultaneous ejection of one of the BS companions and capture of another component. Here, the star's velocity must be sufficient to overcome the SMBH potential barrier (> 750 km s^{-1} [27]) to become an HVS, and the star should avoid destruction by keeping its high velocity on the entire Galactic scale: $p = p_{\rm c}(r_{\rm p}/1\ {\rm mpc})^3 p_{\rm ej}\, p_{\rm s}\, p_{\rm g}$.

3.4 Calculated population of S-stars in the Galaxy

As HVS generation and secondary component capture are considered by one Hills mechanism, their populations should be correlated. This enables us to predict the statistics of S-stars and their mass and semimajor axis distributions in SMBH–S-star binaries. The essential parameter is the HVS ejection velocity $v_{\rm eject}$ (see Section 3.1). The ejection velocity can be used to estimate the energy carried away by the HVS star from the three-body system, and the remaining energy

$$E_{\rm S} = \frac{m_{\rm S} v_{\rm p}^2}{2} - \frac{m_{\rm eject} v_{\rm eject}^2}{2} - \frac{G M_{\rm SMBH} m_{\rm S}}{r_{\rm p}} \tag{5}$$

is spent sustaining the SMBH–S-star pair with the semimajor axis $a = (r_{\rm a} + r_{\rm p})/2$, where $v_{\rm p}$ and $r_{\rm p}$ are the velocity and distance of the captured star at the pericenter (where the HVS is ejected from), and $r_{\rm a}$ is the apocenter distance calculated from the equation of motion

$$\frac{{\rm d}r}{{\rm d}t} = \sqrt{\frac{2}{m_{\rm S}}\big(E_{\rm S} - U(r)\big) - \frac{M^2}{m_{\rm S}^2 r^2}} = 0\,. \tag{6}$$

Here, $m_{\rm eject}$ and $m_{\rm S}$ are the masses of the ejected and captured BS components, $M_{\rm SMBH}$ is the SMBH mass, $U(r)$ is the potential energy of the captured secondary component in the SMBH gravitational field, and M is the angular momentum.

Analyzing the whole statistical ensemble of the initial BS configurations makes it possible to construct the orbital distribution of the secondary BS component captured by the SMBH. For the most probable BS capture generating an HVS, a compact S-star orbit arises with the major semiaxis in the narrow range of $(3-4) \times 10^4 R_\odot$ (Fig. 10) [68]. The orbits of observed S-stars are larger, $A \in (0.2-6) \times 10^6 R_\odot$ [34]. One of the reasons for this discrepancy is likely to be related to the HVS generation condition realized at small $r_{\rm p}$. As a result, the captured component has a more compact orbit. Loosening the ejection condition for arbitrary velocity, not necessarily an HVS, yields wider S-star orbits consistent with observations.

Other reasons for the inconsistency may indicate different S-star formation scenarios. For example, according to

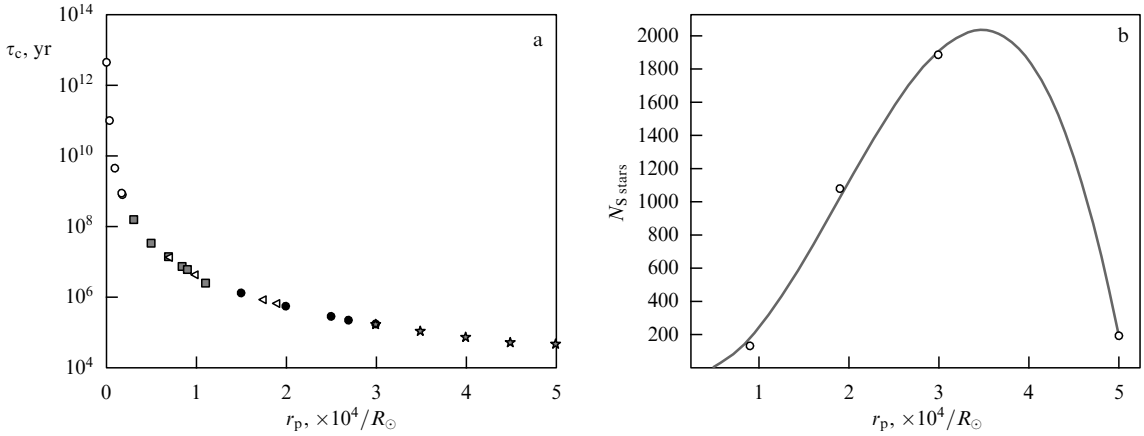

Figure 11. (a) Dependence of BS capture scale by an SMBH ($3.4 \times 10^6 M_\odot$) on r_p [68]. Curve is calculated by modeling 250,000 initial configurations in the N-body formulation [55]. Symbols on the curve correspond to different BS major semiaxes: $A = 11.3R_\odot$ (circles), $A = 56R_\odot$ (filled squares), $A = 125R_\odot$ (triangles), $A = 425R_\odot$ (dark dots), $A = 425R_\odot$ (stars). (b) S-star distribution near the SMBH for surviving BS companions [65] ejected with a velocity > 750 km s^{-1} [27] for the considered BS major semiaxes. Integral under the curve characterizes S-star population accumulated over the Galactic history inside one mpc region around the SMBH and is equal to 2600 [68].

calculations by Loose et al. [69], during natural star formation in the Galactic Center, gas is effectively kept in the deep potential well and is used for star formation. Calculations by Fargione et al. [70] suggest that the origin of S-stars may be related to the tidal stripping of young stellar clusters during their passage near the central SMBH; the young, dense stellar cluster Arches may provide an example.

The destruction of nearby Galactic satellites can also lead to the appearance of central S-stars. Presently, 15 stellar streams have been discovered by the *DES* project [71], which is evidence of activity of such processes. The observational selection effects can also affect the observed distribution on major semiaxes, because stars inside the central 1 mpc have remained unavailable for observation so far.

Numerical calculations in the Hills scenario predict the Galactic Center S-star population from the relation between the time of a binary star capture by the SMBH and the Galactic age (~ 13.6 billion years), provided that an HVS ejection results from the capture. The evolution time of S-stars is determined, as with ordinary stars, by the nuclear burning rate. Magnetic and/or gravitational braking, which could accelerate stellar evolution, are not important evolutionarily [52, 72].

This conclusion is well illustrated by Fig. 11, showing the dependence of the BS capture time on its major semiaxis A and r_p. Here, model statistics on S-stars [68] as obtained from modeling 250,000 initial configurations with a fixed major semiaxis are also presented. This finding required correcting the statistics on S-stars using the selection factor on the major semiaxis, which is estimated as the fraction of model BSs in their total number determined by the initial distribution over A [73–76]. This approach is justified if the A-distribution of stars is the same in both the central Galaxy and solar vicinity.

To take into account the effect of mass segregation of stars on S-star statistics, the mass spectrum was convolved with the lifetime of S-stars, which was assumed to be the same as for main sequence stars. The mass spectrum was taken as the initial mass function (IMF) $\mathrm{d}N \sim M^{-1.35}\mathrm{d}M$ for binary stars in the solar vicinity [77–79] and $\mathrm{d}N \sim M^{-2.35}\mathrm{d}M$ for single stars [80]. Both IMFs give almost identical results (Fig. 12) — only a tiny fraction of BSs could eject HVSs and hence populate the Galactic Center by S-stars over the SMBH

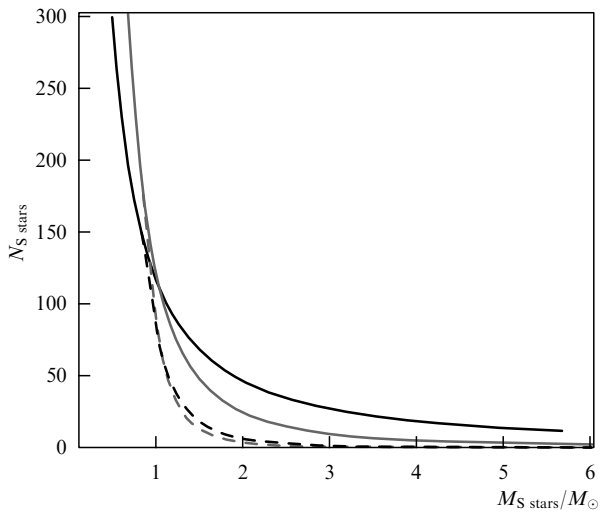

Figure 12. Calculated S-star mass spectra. The black and grey solid curves correspond to the IMF for BSs [73–75] and single stars [80]. The dashed curves show the identical distributions considering the IMF convolution with the lifetime of S-stars.

lifetime. Integrals under the curves in Fig. 12 in the mass interval $(0.5-5)M_\odot$ give the corrected number of S-stars ($\sim 1000-2000$) accumulated over the Galactic lifetime in its center.

S-stars presently observed are classified as B-stars with a mass of $(3-3.5)M_\odot$, corresponding to the theoretical S-star population in this mass interval of 5. It is not surprising that modern observational capabilities do not allow us to discover stars at a distance of one mpc from the center. Interestingly, the Kroupa mass spectrum [81] and the spectrum obtained from observations of the Arches nuclear cluster [70] turn out to be close to the Salpeter mass spectrum [80], which supports the above estimate of the number of S-stars around the SMBH ($r < 1$ mpc).

3.5 Formation probability of hypervelocity stars in the Galaxy

Each formation scenario of HVSs can produce only a fraction of their number. For example, in the model of occasional

capture of binary stars, assuming their population around the SMBH in the 0.1–0.01-pc layer, the HVS formation rate is $\sim 10^{-5} - 10^{-7}$ per year.

Hills derived the geometrical probability of BS capture with major semiaxis $A = 0.01$ a.u. into the SMBH vicinity with a radius of 1 a.u. at $\sim 10^{-4}$ per year, considering that the number of BSs with such A is $\sim 1\%$ of their total number [13]. The capture probability increases by an order of magnitude for wider BSs with $A = 0.1$ a.u. inside 10 a.u. around the SMBH.

By analyzing the HVS formation rate in alternative scenarios, Perets formulated some dynamical and evolutionary constraints on the nature of HVSs [82]. These estimates are based on the idea that HVS formation and the secondary BS component capture should be equally probable. The modeling by Sesana et al. [29] of the *in-spiral* scenario yielded the fraction 0.05 of HVS ejections from 10,000 hypothetical BS captures. In this scenario, stars of the nuclear cluster with a $5000 M_\odot$ black hole are effectively scattered during its spiral-in, 'plunging' toward the Galactic Center bottom with the central SMBH. Based on present-day statistics on Galactic HVSs (~ 100 stars), the number of captured stars into the central 0.01 pc around the SMBH was estimated to be $100/0.05 \sim 2000$ [29, 82]. Taking into account the duration of the flight of an HVS ($\approx 10^8$ mln yr) ejected with a velocity of ~ 1000 km s^{-1} from the Galaxy (~ 100 kpc), Perets estimated the capture probability as $2000/10^8 \approx 2 \times 10^{-5}$ per year. This estimate also corresponds to the HVS formation rate. But the requirement that the central 0.01 pc around the SMBH harbor 2,000 B-stars clearly contradicts the latest observations [31–33].

Analyses of ejection velocities, modeled in the kick scenario of stellar scatterings on a cluster of stellar-mass black holes near the SMBH [19, 28], showed that stellar ejection mainly occurs with velocities < 100 km s^{-1}. Taking into account the proportion of ejections with velocities > 800 km s^{-1} and using the observed number of Galactic HVSs ~ 100 HVS, the number of stars ejected with velocities < 100 km s^{-1} that did not overcome the SMBH gravitational barrier was found to be 18,000, following from $100(100/800)^{-2.5}$ [19, 82].

Considering that the HVS lifetime as a star with a mass of 3–4 $M_\odot$ is about a hundred million years, the HVS formation rate was estimated to be $18{,}000/10^8$ years $\approx 10^{-4}$ stars per year [19]. This is a lower limit, because most stars do not scatter beyond the SMBH vicinity. Assuming this HVS birthrate, the Galaxy should contain around 10^4 HVSs, if the time to fly from the Galaxy is $\sim 10^8$ years. This implies that the HVS density near the Sun is ~ 1 star per cubic kpc^3.

The *in-spiral* [29] and kick-scattering [19, 28] scenarios *a priori* demand a continuous stellar density distribution around the SMBH, which is not supported by observations. Current observations of the central 100-mpc region reveal a cluster of stars with chaotically oriented orbits. The main population consists of very massive young B-stars, and one third is represented by old red giants [31]. The population of this cluster (300–500 stars) does not coincide with the number predicted by different scenarios [19, 28, 29]: it yields an HVS birthrate 100 times as low ($\sim 10^{-6}$ per year), as is well reproduced by the Hills mechanism and estimate of $\sim 10^{-2}$ HVS per cubic kpc^3 around the Sun. Probably, this is a lower estimate because most HVSs can be ejected with high velocities and leave the Galaxy.

The appearance of HVSs in the Galaxy can also be related to their ejections from centers of other galaxies. Such hypothetical ejections, for example, from the nucleus of the Andromeda galaxy, were studied by Sherwin et al. [20] who showed that the Hills scenario can provide ~ 1500 'runaway' stars inside the virialized Galactic halo. Bromley et al. [17] produced a virtual catalog of stars ejected from the Galactic Center, whose trajectories were re-integrated taking into account the Galactic potential. This enabled constructing a virtual HVS galactocentric distribution that can be used to make comparisons to observed and as yet undiscovered HVS.

3.6 Modeling of stars with relativistic velocities

As noted above, the classical Hills scenario constrains the stellar ejection velocity by $0.1c$, which directly follows from the theory of gravitation and black hole physics. Numerous calculations by different authors [16–20, 26, 55, 65, 66] in the three-body and N-body problem formulation support this theoretical conclusion. Summarizing the findings of Section 2.3, we can say that, for each star of mass M_*, there is an SMBH with the limiting mass $M_{\rm cri}$ capable of giving the star the maximum possible gravitational acceleration $a_{\rm cri}$. If this star moves in the vicinity of a more massive SMBH than $M_{\rm cri}$, the kinetic resource for acceleration remains the same. This limitation, however, is relaxed in the case of dynamical capture of a binary system, one of the components of which is also an SMBH (call it the host SMBH). This is the modified Hills scenario. Numerical simulations of this scenario were carried out similarly to calculations in the classical Hills scenario [13].

A 'bank' of arbitrary binary orbits (200,000 initial configurations) was created in the three-body problem formulation. The analysis of the calculated velocities of the ejected stars (Fig. 13) enables us to select those binaries which produced ejection velocities exceeding $0.3c$. Another modeling in the N-body problem formulation was performed for these systems to check the tidal disruption of a star consisting of 4,000 gravitationally bound structural elements. The host and central SMBHs were assumed to be point-like objects.

In simulations in [42], a binary system, including an SMBH with mass $M_2 = 4.5 \times 10^5 M_\odot$ and a star with mass m and radius R, was studied in four variants: ($1M_\odot$; $1R_\odot$), ($2M_\odot$; $1.6R_\odot$), ($3M_\odot$; $2.55R_\odot$), and ($4.5M_\odot$; $3.3R_\odot$). The major semiaxis of the binary system a_2 was determined from the analysis of the tidal radius of the star in the host SMBH field. The fall of the binary towards the central SMBH ($M_1 = 4.5 \times 10^6 M_\odot$) in an elliptical orbit with an apocenter of $10^5 R_\odot$ and pericenter of $r_{\rm p}$, estimated from the disruption condition of the binary system components, $r_{\rm p} < 2^{4/3} a_2 \times [M_1/(m + M_2)]^{1/3}$, was calculated. The orbits were numerically integrated in the Newtonian mechanics using the velocity Verlet–Weis algorithm [56].

The change in the specific total energy of the star over one orbital revolution around the central SMBH enables identifying the ejection event for a given energy increase. Otherwise, additional estimates of the specific binding energy of the star with the host and central SMBH are needed to distinguish the dynamical 're-capture' of the star by the central SMBH. The model ensemble of the initial three-body configurations provided a statistically significant number of HVSs with relativistic velocities, dynamical 're-captures', and so-called drifting ejections when the energy is insufficient for the ejection but the star gets unbound from two SMBHs and freely drifts in their surroundings [42].

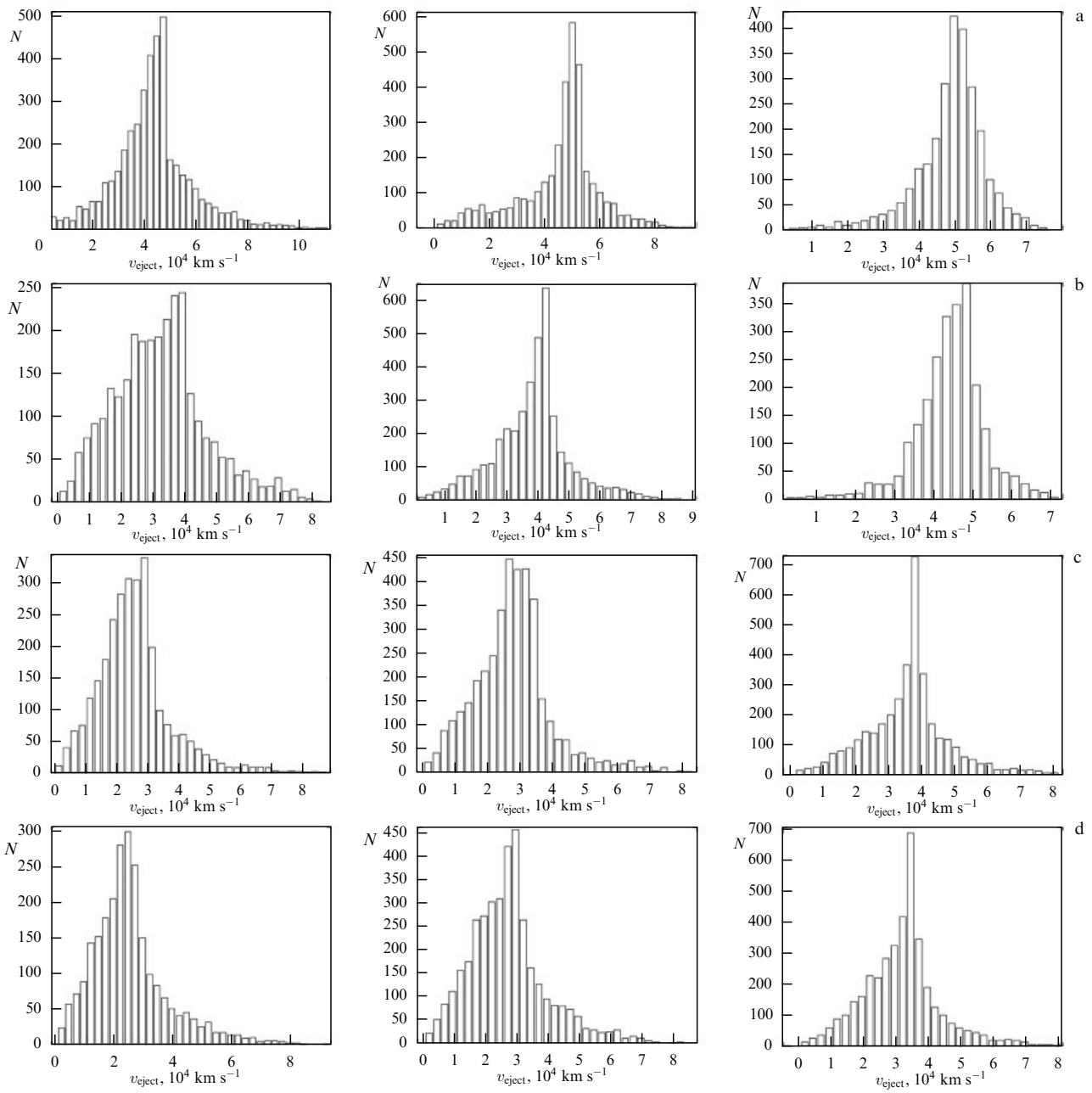

Figure 13. Velocity spectra as calculated in the modified Hills scenario in the three-body problem formulation. Calculations for a binary system consisting of an SMBH ($4.5 \times 10^5 M_\odot$) and a star passing near the central SMBH ($4.5 \times 10^6 M_\odot$). Each row corresponds to the star's mass $1M_\odot$ (a), $2M_\odot$ (b), $3M_\odot$ (c), and $4.5M_\odot$ (d). Three plots in a row correspond to $r_{\rm p}$ $100R_\odot$, $150R_\odot$, $250R_\odot$ (from left to right).

The ejected star velocity distributions depending on its mass can be used to estimate the maximal and mean ejection velocities (Fig. 13). A tendency toward increasing maximal ejection velocity with decreasing stellar mass and $r_{\rm p}$ can be seen (Fig. 14).

Note that the tidal radius of a star with mass $1M_\odot$, $2M_\odot$, $3M_\odot$, $4.5M_\odot$ in the central SMBH field is $208R_\odot$, $264R_\odot$, $367R_\odot$, and $416R_\odot$, respectively. Maximum ejection velocities were reached at much closer passages, which can disrupt the star by the tidal field of both SMBHs.

Numerical experiments [42] done for a $1M_\odot$ star show that, when passing near the SMBH at a distance of $100R_\odot$ in 87 trials, the three-body calculations led to an ejection velocity of above 80,000 km s^{-1}. N-body calculations confirmed the ejection without disruption. This means that the probability of ejecting a $1M_\odot$ star with a relativistic velocity from 10^4 initial orbital configurations with $r_{\rm p} = 100R_\odot$ is ~ 0.008.

The same statistical ensemble, calculated for orbits with $r_{\rm p} = 150R_\odot$, yields only 20 relativistic ejections confirmed by N-body calculations, which decreases the relativistic ejection probability by a factor of four. With increasing pericenter distance, relativistic ejections of stars become rare and disappear altogether. With increasing stellar mass, the probability of ejection with a relativistic velocity ($>80{,}000$ km s^{-1}) sharply decreases to zero.

Undoubtedly, we are dealing with a rare random event that requires a combination of factors, including a low stellar mass and the star's ability to penetrate under the tidal radius. In these calculations, the maximum impact parameter $\beta = r_{\rm t}/r_{\rm p}$ was 1.55 and 2.7 during passages near the central

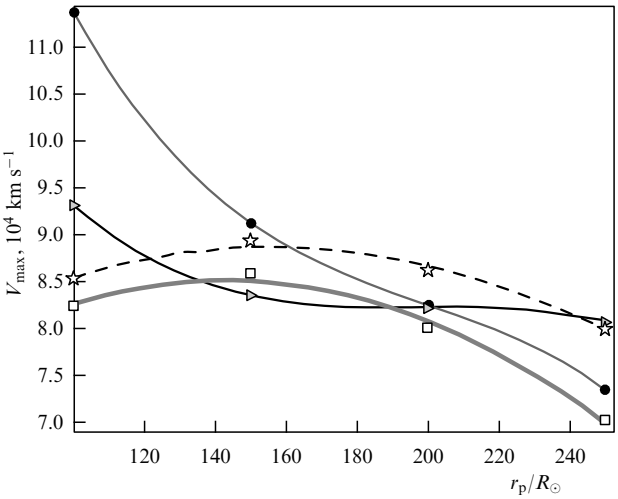

Figure 14. Maximal ejection velocity V_{max} of a star as a function of its mass and r_p obtained in the modified Hills scenario in the three-body problem formulation. Calculations for a binary system consisting of an SMBH ($4.5 \times 10^5 M_\odot$) and a star passing near the central SMBH ($4.5 \times 10^6 M_\odot$). Four masses of the star correspond to $1M_\odot$ (dots), $2M_\odot$ (squares), $3M_\odot$ (stars), and $4.5M_\odot$ (triangles).

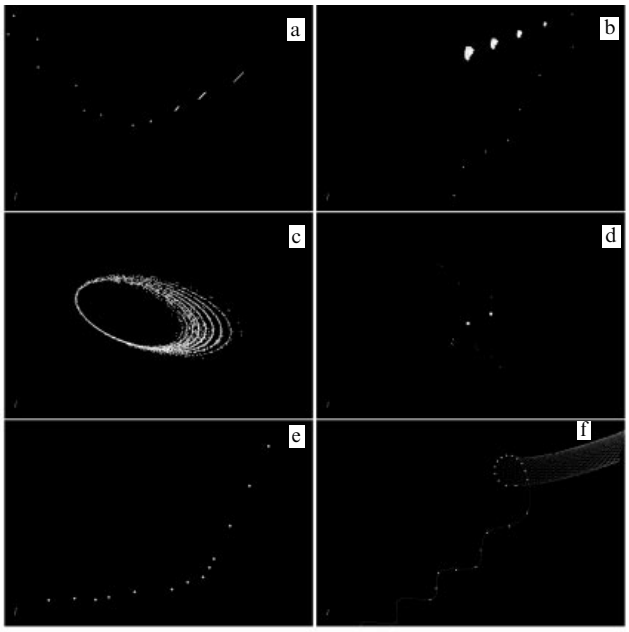

Figure 15. Parts of the orbital flyby of a binary system consisting of a star and the host SMBH ($4.5 \times 10^5 M_\odot$) near the central SMBH ($4.5 \times 10^6 M_\odot$). (a, b) Dynamics of the disruption of a star ($1M_\odot$) passing at $r_p = 50R_\odot$ ($\beta = 4$). (c) Disk 'trace' of the disrupted star ($1M_\odot$) around the central SMBH after flyby at $r_p = 200R_\odot$ ($\beta = 1$). (d) Fragmentation of star ($1M_\odot$) in two parts during its passage at $r_p = 150R_\odot$ ($\beta = 1.3$); in the gravitational model ignoring gas dynamics, this outcome is interpreted as disruption. (e) Ejection of a star from $1M_\odot$ with $r_p = 100R_\odot$. (f) Dynamical re-capture of a star ($4.5M_\odot$) by the central SMBH at $r_p = 1000R_\odot$. All plots are shown for a star consisting of N elements. Before pericenter passage, the star's trajectory is sine-like, indicating the presence of an invisible host SMBH.

and host SMBH, respectively. Figure 15 shows parts of orbital passages for different orbital configurations from a set of events with stellar disruptions, ejections, and dynamical re-captures by the central SMBH. For 200,000 initial orbital configurations, the probability of ejection with a relativistic velocity is 5.5×10^{-4} [42]. The next step is to estimate the realization probability of the calculated statistics.

3.7 Formation probability of relativistic velocity stars in the Universe

The modified Hills scenario explains the origin of relativistic stellar velocities. But what is the reason for this mechanism? Of the three bodies involved in the redistribution of kinetic energy, two are nonclassical SMBHs. They suggest the answer: galaxy clusters or groups are required for the Hills mechanism to operate, where collisions and mergings of galaxies accompanied by encounters and coalescences of their central parts populated by SMBHs occur. It should be stressed that galaxy mergings in groups are more effective for central passages due to small relative distances and velocities as compared to such processes in galaxy clusters. This idea is supported by numerous observations of merging galaxies [44] and model calculations of their merging rate [83]. The birth of stars with relativistic velocities is impossible in our Galaxy due to firmly established Keplerian orbits of S-stars around the single SMBH. However, the appearance of such stars as intergalactic 'runaway' stars is not ruled out.

Let us estimate the collision rate of galaxies by assuming that each of them harbors an SMBH. In collisional processes, the galaxy encounter rate is determined by their free-path length, which can be estimated as the ratio of the galactic volume $V = (4/3)\pi r^3/N$ to the effective scattering cross section $S_{eff} = \pi(2r_{eff})^2$. Here, r is the radius of a cluster or group, N is the number of galaxies in the cluster (group), and r_{eff} is the radius of the effective flyby of galaxies at which the galaxies should pass relative to each other to eject stars with relativistic velocities.

Model experiments with the modified Hills scenario [42] estimated r_{eff} to be $(7-10)\, r^1_{sch}$, where r^1_{sch} is the Schwarzschild radius of the central SMBH. Then, the effective scattering cross section is $S_{eff} = 2.25 \times 10^{-5}$ pc^2. For a typical galaxy cluster with $N \sim 1000$ and $r = 3$ Mpc, the free-path length is $\lambda \sim 5 \times 10^{21}$ pc, while, for a group of galaxies ($N \sim 50$, $r \sim 1$ Mpc), it is $\lambda \sim 3.7 \times 10^{21}$ pc.

Assuming the velocity dispersion of galaxies in a cluster or group $\sigma_V \sim 1500$ km s^{-1} or ~ 150 km s^{-1}, we can estimate the time between two consecutive encounters $\tau = \lambda/\sigma_V$, which is 5×10^{24} yr and $\sim 2.5 \times 10^{25}$ yr for clusters and groups, respectively. Considering that these estimates are obtained for a single encounter of galaxies, the mean time between two consecutive collisions among all possible galactic pairs in a cluster or group is $\langle\tau\rangle = \tau/N_{pair}$. Modern estimates of the number of clusters and groups are very approximate, $\sim 10^9$ and 4×10^{10}, respectively. From the number of possible pairs in all galactic groups, $N_{pair} \sim 50^2/2 \times (4 \times 10^{10})$, we then obtain $\sim 5 \times 10^{13}$ combinations, and in clusters, 20 times as high, i.e. $N_{pair} \sim (1000^2/2) \times 10^9 \sim 10^{15}$. Thus, the mean time between collisions of all possible pairs in galaxy groups and clusters is $\langle\tau\rangle \sim 2 \times 10^{11}$ and $\langle\tau\rangle \sim 10^{10}$ years, respectively. This estimate is comparable to the age of the Universe for clusters and exceeds the age of the Universe by ten times for groups. But low relative velocities of galaxies in groups may indicate nonrectilinear motion, significantly increasing the collision probability with the required parameters.

The need for effective passaging at a distance of (7–10) r^1_{sch} to produce a relativistic ejection makes such events rare. The statistics on rare events suggests that they happen in groups. Let us consider how, in our problem, a suite of relativistic ejections can be generated.

Dynamical braking leads to a concentration of the most massive stars at the center of a galaxy. A black hole appears that gradually assembles stars in a nuclear cluster and increases mass on a dynamical time scale of the nuclear cluster of $\sim 10^8$ years. Subsequent mass growth occurs on the Hubble time scale due to occasional flybys of galactic single or binary stars and stellar clusters. These processes reserve central S-stars for possible ejections, including relativistic ones. When galaxies pass through each other with a central impact parameter of (7–10) $r^1_{\rm sch}$, each captures stars of the neighbor galaxy into its effective scattering radius. The number of such stars 'raked up' at the front of the galaxy's motion can be estimated from the ratio of the mean galactic radius to the swept area. Assuming that the central number density of stars is as in the Galactic Center, $\sim 8 \times 10^7$ pc^{-3}, and using the above estimate of $S_{\rm eff}$, we can conclude that up to 10 mln stars can be collected in the S-star region. They are potential candidates for stellar ejections with relativistic velocities [45].

Using 200,000 trial calculations in the modified Hills scenario, we estimate the probability of relativistic ejections as 5.5×10^{-4} [42]. Therefore, from the total sample of S-stars ($\sim 10^7$), the number of possible relativistic stellar ejections is about several thousand. Such a 'relativistic fountain' is possible from a single collision of two galaxies, provided that their central parts with SMBHs pass by a distance of (7–10) $r^1_{\rm sch}$. In these estimates, we assumed that the mass of one SMBH is $10^9 M_\odot$, as in the Virgo cluster. Note that these calculations ignored stars less massive than $1 M_\odot$, which scatter more efficiently with relativistic velocities. Thus, the obtained number of relativistic ejections ($\sim$ 10,000) is the lower limit. This result encourages a search for stars with relativistic kinematics.

4. Discovery of S-stars

4.1 Early evidence of a supermassive black hole in the Galactic Center

One of the first pieces of observational evidence of an invisible mass in the Galactic Center was obtained in 1980 by Lacy et al. [84] from near-IR ($\lambda = 12.8$ μm) measurements of the radial velocity of ionized Ne II-gas localized in clouds moving along orbital segments close to circular orbits. Later, a suite of spectral studies of the 4-pc region around Sgr A* was performed that enabled imaging all flows of the ionized gas, which appeared as one common stream, the so-called one-arm minispiral moving out of the center at a distance of 1–3 pc [10]. Consequently, the minispiral was reproduced by Fridman and Yanchenko [85] in numerical modeling of the super-reflection instability developed in the disk.

The spiral motion rejected the idea of an explosive gas outflow and was approximated by a Keplerian rotational curve around a central mass of $2 \times 10^6 M_\odot$ concentrated inside 0.1 pc around Sgr A*. Considering the present estimate to the Galactic Center of 8.32 kpc [34], the size of this region corresponds to $\sim 3''$ arcsec — in the 1980s, this was the limiting angular resolution.

Another indirect confirmation of an invisible mass in the Galactic Center was obtained by McGinn et al. [11] from the kinematical analysis of stars within the central 8-pc region, which were spectroscopically studied in the near IR ($\lambda = 2.3$ μm) on the CO absorption line. The mean radial velocity and velocity dispersion were measured as a function of the galactocentric distance. They were used to independently estimate the invisible mass of $\sim 4 \times 10^6 M_\odot$ localized in the central stellar cluster. In addition, paper [11] studied the radial dependence of the mass ratio inside the central region of radius r, toward the CO absorption intensity ($M_{\rm r}/F_{\rm K}$), on the galactocentric distance, which increases toward the center. One of the possible reasons for such an increase could be the decrease in the CO absorption intensity related, for example, to a changing stellar population. This behavior could be explained if, at 0.6 pc from the center, dwarfs of the late spectral class, instead of giants, dominate. However, a contradiction arises: due to dynamical friction [30], more massive objects populate the Galactic Center first. Of course, the main problem is the central mass $M_{\rm r}$, which dwarfs cannot explain. Therefore, the authors of [11] proposed that the main candidate for the invisible mass is a cluster of neutron stars or a single object like an SMBH.

4.2 Projects of long-term monitoring of the Galactic Center. Methods of observations

In the 1970s, the assumption was put forward that the centers of all galaxies without exception harbor SMBHs irrespective of their nuclear activity [4]. An intriguing instance was the 'quiet', relatively close nucleus of our Galaxy and the possibility of its exploration. At that time, two huge projects to monitor the central region inside one arcsecond to search for S-stars were planned.

The first one was headed by the European Southern Observatory (ESO) and started in 1989 using the 3.5-m New Technology Telescope (NTT) (La Silla, Chile). Since 1992, it has continued with the Very Large Telescope (VLT) (Sierro Paranal, Chile). The second project started in the same year using the 10-m Keck telescope (Hawaii) run by the University of California. From observations on the 3.5-m NTT-3.5-m telescope, Eckart and Genzel [12] measured the proper motions and radial velocities of 39 stars localized in the layers 0.04 pc $< r <$ 0.4 pc. Using these measurements, they calculated velocity dispersions that increased to the center. This distribution suggested an object with a mass of $2.5 \times 10^6 M_\odot$ localized inside 0.015 pc around the radio source Sgr A* and the mean velocity field isotropy.

Adaptive optics technology in the near IR ($\lambda = 2$ μm) enabled taking and measuring digital images of S-stars with a higher angular resolution than available from speckle-interferometry. Using the SHARP speckle-camera instead of the NACO (NAos-COnica) photodetector, the spectral resolution accuracy increased by a factor of eight. This enabled reconstructing the 3D structure and parameters of the orbits of S-stars. Jointly with spectral data, this information helped in recovering the gravitational potential in which the S-stars move as probe masses and the position of the center of mass.

Additional control of the localization of the invisible object is obtained from infrared flares of SiO-masers observed from the Galactic Center. The improved localization of the flares is well correlated with the position of the radio source Sgr A* [86]. All data are consistent within one arc ms (8.32 a.u.) and in best agreement with the source localization determined by the statistical parallaxes of clusters [87].

4.3 First orbit of the star S2. Progress in the study of S-stars

Progress in astronomical techniques has helped the rapid growth of S-star statistics:

• by 2002, the first orbit of an S-star (S2 on the list of the VLT program) was measured, which turned out to be very convenient for finding orbital parameters. S2 has $+14^m$ in the K-band and orbital period $P_{\rm orb} \approx 15.9$ years. S2's orbit is measured very well, and the joint NTT/Keck data yield the SMBH mass and location $M_{\rm SMBH} = (4.35 \pm 0.13) \times 10^6 M_\odot$ and $R_0 = 8.33 \pm 0.12$ kpc [34]. The orbital solution for S2, obtained taking into account GR effects, does not differ significantly from the Keplerian solution: $M_{\rm SMBH} = (4.43 \pm 0.14) \times 10^6 M_\odot$ and $R_0 = 8.41 \pm 0.13$ kpc [34];

• by 2005, the orbits of five of ten observed S-stars were measured [14] using the new integral field spectrograph, SINFONI (Spectrograph for INtegral Field Observations in the Near Infrared) [88];

• by 2009, the orbits of 28 of 109 S-stars had been measured using modified adaptive optics instruments. The results of two independent teams at VLT and Keck are in good agreement on the SMBH mass and distance: $R_0 = 8.31 \pm 0.33$ kpc, $M_{\rm SMBH} = (4.29 \pm 0.07) \times 10^6 M_\odot$ [89] and $R_0 = 8.4 \pm 0.4$ kpc $M_{\rm SMBH} = (4.5 \pm 0.4) \times 10^6 M_\odot$ [90];

• by 2018, the orbits of 47 of 200 monitored stars had been measured by the infrared interferometer GRAVITY installed on four VLT telescopes (30 micro arcsec), enabling a 16-fold gain in spectral resolution compared to NACO;

• in 2020, the closest star to an SMBH, S62, with a pericenter distance of ~ 16.7 a.u., $+16^m$ in the K band, and $P_{\rm orb} \approx 9.9$ years, was found [92]. The orbital solution for this star from the VLT and Keck observations constrains the SMBH mass to $(4.15 \pm 0.6) \times 10^6 M_\odot$.

Of all known S-stars, the orbits for 17 were selected by gravitational acceleration to perform multi-star orbital fitting (Fig. 8 from [34]). The description of the orbits of 17 stars has 109 free parameters: seven describe the SMBH, including its sky location (α, δ), three velocity components (v_α, v_δ, v_z), the mass and distance ($M_{\rm SMBH}$, R_0), and 6 orbital parameters describe the S-star (major semiaxis, eccentricity, orbital inclination, moment of periastron passage, and ascending node longitude). The best solution yields $M_{\rm SMBH} = (4.28 \pm 0.103) \times 10^6 M_\odot$ and $R_0 = 8.32 \pm 0.07$ kpc [34]. Here, the systematic and statistical errors are almost half those for the paper results [89].

4.4 Prospects for GR testing in the strong gravity regime

Observations of S-star orbits collected over 30 years offer a unique test of relativistic effects of Special Relativity and GR in the strong gravity regime (millions of solar masses), which has not been probed so far in the Solar System. Now, there are two candidates with high relativistic factor β: S2 (0.0255), which has already passed the pericenter with a velocity of ~ 7650 km s^{-1} [91, 93], and S62 (0.1), which will pass the pericenter in February 2023 [92]. Their relativistic orbits can be used to test several effects.

(1) The Schwarzschild precession (GR effect) — turn of the S-star orbit in the orbital plane. The effect in curved space-time is similar to the relativistic apse motion in eccentric binary systems.

(2) The gravitational redshift (GR effect). The radiation frequency shift near a massive body due to time retardation in the body's gravitational field.

(3) The transversal Doppler effect (SR effect). The radiation redshift due to time retardation in the frames moving normal to the line of sight with a relativistic velocity. For S2, the observational accuracy is insufficient to separate the gravitational redshift from the transversal Doppler effect. The total effect changes the pericenter and apocenter velocity by 200 km s^{-1} and 6 km s^{-1}, respectively [91].

(4) The Roemer time delay (SR effect). Light from a star from different orbital points reaches the observer with a delay due to the finite velocity of light (eight days over the orbital period for S2).

(5) The Shapiro effect (joint SR and GR effect). Due to light bending in the gravitational field of a massive object and the finite speed of light, the uncertainty of a star's position in orbit emerges (20 arc ms for S2 [91]).

(6) The Lense–Tirring effect (GR effect). The entrainment of the reference frame by a rotating body, SMBH; the impossibility of being at rest inside the ergosphere of a rotating black hole. The orbital wobbling of S2 would be 9 arcseconds [91], beyond present observational capabilities. S-stars closer to the SMBH than S2 are needed to measure this effect.

(7) The quadrupole mass moment, the consequence of a nonzero spin of the SMBH. It can be detected from precise measurements of the motion of S-stars with semimajor orbital axes smaller than one mpc, from gravitational wave detections generated during the spiral-in of a stellar-mass object, and from measurements of the SMBH shadow [94, 95].

(8) The local space invariance (part of the more general Einstein equivalence principle of GR). It states the independence of nongravitational measurements on the spatial location. The international GRAVITY collaboration estimated the change in H and He line frequencies at different orbital points of S2 $(2.4 \pm 5.1) \times 10^{-2}$, consistent with zero within the measurement error [96].

Thus, for the first time, GR testing was carried out in a gravitational field one order of magnitude stronger than the field of white dwarfs and six orders of magnitude stronger than Earth's gravitational potential.

4.5 Direct confirmation of the supermassive black hole in the Galactic Center

Presently, the radio source Sgr A* discovered in 1974 [97] is ultimately identified with an SMBH. Studying the dynamics of two dozen S-stars allowed us to put stringent and direct constraints on the nature of the SMBH [34]. The most reliable parameters were obtained from the S2 orbital fitting from VLTI (Very Large Telescope Interferometer) GRAVITY near-infrared observations that yield the best SMBH mass estimate $M_{\rm SMBH} = (4.148 \pm 0.014) \times 10^6 M_\odot$ (with a $\sim 0.34\%$ error) [98]. The distance to the SMBH is $R_0 = 8178$ pc with an error of 13 pc (0.16%) due to radial velocity uncertainties and 22 pc from the astrometric calibration uncertainty [98].

The next precisely measured star is S1. Despite its long orbital period of ~ 166 years, of which S1 has so far covered less than π of the orbital phase, its error ellipse is smaller than for other S-stars, yielding the SMBH distance and mass $R_0 = 8470 \pm 180$ pc (2.1%) and $M_{\rm SMBH} = 4.45 \pm 0.28 M_\odot$ ($\sim 6.3\%$), respectively [34].

Even larger uncertainties in SMBH mass and distance estimates have been obtained for S9 and S13: $R_0 = 8080 \pm 780$ pc (9.6%), $M_{\rm SMBH} = 4.04 \pm 1.26 M_\odot$ ($\sim 30\%$) and $R_0 = 8740 \pm 970$ pc (11%), $M_{\rm SMBH} = 4.84 \pm 1.59 M_\odot$ ($\sim 33\%$), respectively [34].

S55 is the S-star with the shortest orbital period. However, its orbital parameters cannot be derived, because its radial velocity is constant at $+50$ km s^{-1} [34]. In the nearest future, the SMBH spin can be measured. If nonzero,

it should be imprinted in the motion of S-stars and plasma emission.

Other independent evidence of SMBHs can be obtained from an analysis of long-term monitoring of the motion of gas clouds G2/G1 by SINFONI and Chandra X-ray observations [99]. The astrometric trajectory of the clouds reveals their spiral orbital motion. Also, radio and sub-mm polarization observations constrain the gas accretion rate from the clouds onto the SMBH: $(10^{-9}-10^{-7})M_{\odot}$ yr^{-1} at a distance of $(10-100)\,r_{\rm sch}$ [100] and $\sim 10^{-5}M_{\odot}$ yr^{-1} at a distance of $1000\,r_{\rm sch}$ [101]. This low accretion rate and the small value of the Eddington factor 10^{-8}, which is the ratio of the emission power from Sgr A* ($50L_{\odot}$) to the SMBH mass ($4.1\times 10^{6}M_{\odot}$) as inferred from the S-star dynamics [98], enables us to treat the SMBH in our Galactic Center as 'underfed'. However, the so-called Fermi bubbles discovered in 2010 suggest a previous explosive quasar phase in Galactic history.

Far infrared (100–160 μm) observations of Sgr A* by the Hershel Space Telescope [103] provide yet another confirmation of the presence of an SMBH in the Galactic Center. The authors of [103] detected the infrared variability of Sgr A* and associated it with SMBH accretion activity with a period of 40 hours.

Despite discovering an ever-growing number of central stars, no more than two dozen S-stars remain informationally valuable, which is surprisingly close to the number of HVSs found so far at the Galactic periphery.

5. Discovery of hypervelocity stars

5.1 History of the first HVS discovery

There are many examples of accidental discoveries in history, and HVSs are no exception. The completion of the first Sloan Digital Sky Survey (SDS) (2000–2003, [104]) offered photometric measurements of several million stars, including at the Galactic periphery. These data enabled studying the detailed kinematic structure of the Galaxy and estimating its dynamical mass.

Among the many scientists who have investigated this problem, Brown and colleagues [15] selected 36 faint high-latitude stars using the color criterion by Yanny et al. [105] corresponding to 'hot' A-stars of the blue horizontal branch. A spectral study of these stars was carried out in the range of 3600–4500 Å by the 6.5-m Multi Mirror Telescope (MTT) equipped with a high-resolution spectrograph (1 Å). From the measured spectra, radial velocities were derived and corrected for the galactic rest standard. The distribution of these radial velocities revealed a 6σ-outlier for one of the stars, SDSS J090745.0 + 024507, with a Galactocentric velocity of 708 km s^{-1}, while the mean velocity and the velocity dispersion of the sample were -7 km s^{-1} and 120 km s^{-1}, typical for the halo stellar population [15]. Subsequent multispectral MMT observations ruled out measurement errors.

The high velocity of SDSS J090745.0 + 024507 cannot be explained by binarity, lacking a systematic velocity shift, or by its origin in the Local Galaxy Group or the Sagittarius stellar stream. The object found is unlikely to belong to the stellar velocity 'tail'; the sample is too small. Stellar ejections due to a supernova explosion in a binary system or pair collisions have a maximal velocity of ~ 300 km s^{-1}, much slower than measured. The Hills scenario is plausible but requires the proper motion measurements.

In 2005, Brown et al. calculated what should be the proper motion of HVS $+19.81^{m}$ at a distance of 55 kpc to confirm the ejection scenario, ~ 0.3 marcsec per year^{-1}. A radial velocity analysis shows that it is directed 180° away from the Galactic Center. The latest Gaia measurements yield the proper motion components $\mu_{\alpha}=-1.012\pm 1.321$; $\mu_{\delta}=-0.269\pm 0.879$ marcsec year^{-1} [36].

The photometry of SDSS J090745.0 + 024507 [15] enabled preliminary conclusions about the star's physical properties to be made. For example, the color indexes correspond to a star on the blue horizontal branch. A late-B (B9.2) main-sequence star with an effective temperature of $\sim$ 10,500 K [15] cannot be ruled out either. The metallicity measured from the equivalent width of the Ca II K line proved to be uncertain, $[{\rm Fe/H}]=-0.4-0$, but allows the solar abundance. The spectral class uncertainty strongly affects mass and luminosity estimates and the distance to the star (39–71 kpc). It took some time to perform and process further observations to understand the physical properties of this star. But the most essential element was the need for a strategy to successfully look for new HVS candidates.

5.2 Method of survey searches in photometric catalogs

According to calculations [13, 16–20, 26, 55, 66], for an HVS birthrate of 10^{-6} per year and the time it takes for the star to fly outside the halo (≈ 100 kpc) of $\sim 10^{8}$ years, the Galactic number of HVSs is ~ 100 stars, i.e., the mean distance between such stars in the solar neighborhood is ~ 5 kpc. Clearly, these are rare objects requiring dedicated searches.

Presently, HVSs are routinely searched for in some space programs that use survey search algorithms among field stars and remote subsystems, for example, in the halo, where the first HVS was discovered. The search algorithm uses Yanny's color criterion [105] to distinguish 'internally hot' stars against the background halo population, which are HVS candidates. The SDSS 4th release with a certain system of color filters [106], which can be called *low-group* spectroscopy, enabled localizing a region containing 430 late-B stars [107]. Spectroscopic observations were used to determine their status. The HVS search algorithm compares the spatial velocity, the lower limit given by the radial velocity, with the Galactic escape velocity at the star's location.

In 2006, another five HVSs were discovered by dedicated searches. Recent spectroscopic surveys of northern B-stars with the MMT include 21 objects unbound with the Galaxy with reliably determined photometric and spectroscopic parameters [37]. We analyze them in detail in Section 5.3.

Another HVS search strategy is based on measurements of their proper motion. Dwarf G–K-stars are studied using this method. However, such low-massive stars are difficult to select spectroscopically. Therefore, as in the case of the halo, the photometric selection using color criteria by Yanny et al. [108] is applied.

These criteria were applied to the SEGUE (Sloan Extension for Galactic Understanding and Exploration) catalog from the SDSS 9th release by Palladino et al. [109], who selected G–K dwarfs with spectroscopically determined metallicity, effective temperature, and free-fall acceleration. By using the isochron diagram calculated for model evolutionary tracks for the found metallicity, it is possible to reconstruct the luminosity and distance to the dwarf. Knowing the distance and proper motion enable determining the tangential velocity, comparable or even higher than the radial velocity, as confirmed by the results in [109].

Comparing the dwarf's space velocity with the Galactic escape velocity gives the kinematic status of the star.

This method enabled Palladino et al. [109] to catalogue 20 HVS candidates among G–K dwarfs. The authors of [109] stressed the large errors in the proper motion measurements, although the stars are located at a distance of 1–6 kpc, much closer than halo B-stars (50–120 kpc). None of the reconstructed orbits of the ejected stars was found to pass through the Galactic Center.

In 2015, a similar search was done by Li et al. [110] using the first release of the regular spectroscopic survey LAMOST (Large Sky Area Multi-Object Fibre Spectroscopic Telescope) [111] jointly with the proper motions from catalogs SDSS-USNO-B (United States Naval Observatory, 'B' catalog is a continuation of 'A' catalog of astrometric standards) [112]. As a result, of more than one million objects, 19 low-mass late F-, G-, and K-stars were selected as HVS candidates. In Section 5.4, we return to discussing the reliability of HVS classification in all the catalogs mentioned above.

Thus, there are two methods of searching for HVSs. First, it is possible to search for them among bright halo stars that contrast with the local old globular cluster population and, therefore, likely arrived in the halo with high velocities, because the duration of the light should be consistent with the age. Second, it is possible to conduct survey observations of nearby low-mass disk stars, which are the most numerous. The HVS sample is poor so far but still enables making some conclusions on their nature and origin.

5.3 MMT-catalog of hypervelocity stars

After almost a decade after the discovery of the first HVS [15], a catalog composed by Brown et al. [37] appeared containing the results of spectroscopic observations of 1127 late B-type stars from the SDSS catalog [113]. A comparison of the radial and escape velocities revealed 21 HVSs. The spectroscopic 6.5-m MMT observations yielded the MMT catalog of hypervelocity stars [37].

The Galactic potential and the distance to the star, the latter of which depends on its evolutionary status, should be known in order to estimate the escape velocity. The evolutionary nature of an HVS is obtained from analyzing the model stellar atmospheres [114], which are used to calculate synthetic spectra for best fitting with the observed spectrum of the star. The parameters are the effective temperature and free-fall acceleration. Evolutionary stellar models with a chemical composition corresponding to the star's metallicity are used to estimate the stellar age (the time parameter), which enables recovering other physical characteristics, including the mass and luminosity; the latter is needed to determine the distance to the star.

The position of HVSs on evolutionary diagrams corresponds to main-sequence stars. High rotational velocities (>100 km s^{-1}) obtained from fitting the stellar atmosphere support this conclusion. The masses of the discovered HVSs are $(2.5-4)M_{\odot}$, the effective temperatures vary in the range of 10,380–14,547 K, and the free-fall acceleration is $3.75 < \lg g < 4.62$. The age of these stars (180–400 mln years) exceeds the time it takes to fly from the Galactic Center (66–220 mln years) calculated by integrating back in time the trajectory of the ejected star from its present location at 50–120 kpc [37]. These estimates are consistent with the Hills mechanism of HVS ejections from the Galactic Center [13].

Anisotropy in the HVS space distribution can be noted: 11 of 21 stars are localized towards the Leo constellation and occupy less than 5% of the survey area. However, as the MMT survey was conducted for the northern sky only, the anisotropy should be confirmed. This effect is possibly due to absorption by dust clouds in the solar vicinity. Moreover, the Galactic potential anisotropy can be important: stars ejected along its large semiaxis are decelerated less than those ejected along its small semiaxis [115].

On the other hand, ejections of stars in one direction are possible if their captured host binary systems belong to a regular orbital subsystem. This could provide a similar flight angle and an ejection angle turned by almost 180°, forming something like the HVS 'pathway'. Observations show that all discovered HVSs are localized in two thin disks. The orientation of one of them is consistent with the plane containing the central 'minispiral'; the plane of the other disk coincides with the orbital plane of O–B stars populating nuclear stellar clusters inside 0.5 pc from the SMBH and oriented clockwise [116].

The HVS MMT catalog [37] contains the proper motion components (μ_α, μ_δ) calculated for the assumed central ejection, which can be compared with future Gaia measurements. Now, the Gaia experiment has attained the planned measurement accuracy (0.035–0.17 mas yr^{-1} [37]). Therefore, it is interesting to compare the new proper motion measurements, which could eliminate the uncertainty between the disk and central origin of the HVS.

5.4 Gaia space telescope and the open catalog of hypervelocity stars

The Gaia astrometric mission opened a new era in the 3D mapping of ~ 1.7 billion stars with an unprecedented measurement accuracy in distance (~ 0.3 mas) and proper motion (<1 mas yr^{-1}) [117–119]. Moreover, its rich statistics revealed whole structures formed due to violent dynamical processes, such as the collision of our Galaxy with the Sagittarius galaxy 300–900 mln years ago [120], stellar tidal streams of external stars, and, of course, HVS 'itineraries' [119].

The origin of fast stars is on the list of Gaia observations. For example, astrometric solutions for almost two million stars collected in the joint Gaia–Tycho catalog were used to test the learning matrix composed using the MMT HVS catalog [37]. The matrix was inserted into an artificial neuron network that enabled testing rare object recognition algorithms in big data, like the Gaia–Tycho catalog [39]. The significant number of statistics and minor measurement errors optimistically predicted that, by the end of 2018, thousands of new HVSs could be discovered inside 10 kpc with masses of $1-10M_{\odot}$ and a proper motion relative error of less than 1% [39].

The revision of the astrometric data after Gaia DR2 (Data Release 2) showed that almost all HVS candidates, at least from late F–K dwarfs or giants, are bound to the Galaxy. Most candidates from the Palladino et al. [109] catalog proved to be high-velocity halo stars, and for other stars, erroneous proper motions obtained by ground-based instruments were used. Thus, none of the HVS candidates from [109] have been confirmed.

As for the late-type HVS catalog by Li et al. [110], of 19 candidates, only one object, Li10, was confirmed. It is an F9 dwarf with a galactocentric velocity of 643 ± 93 km s^{-1}. The orbit of Li10 reconstructed in the Galactic potential by Bovy [121] passes at a distance of a few kpc from the Galactic

Center, thus excluding the Hills scenario. Probably, the ejection was due to the disruption of a binary system after a supernova explosion. Although no compact object has been found within 45 arcsec from Li10, this formation channel is plausible for other HVSs with atmospheres enriched with intermediate nuclear burning elements. For example, such are the helium O-subdwarf US708 [122–124] and the white dwarf GD492 [125, 126], which is the hypervelocity compact object closest to the Sun ($\sim$ 632 pc, [127]).

The new Gaia DR2 data forced the previous HVS candidates to be revised. According to [122], for a sample of 20 stars unbound with the Galaxy at a confidence level of more than 80%, 7 stars are 'hyper-runaway' stars, i.e., ejected from the Galactic disk. The other 13 unbound stars are likely to have an extragalactic origin, being single ejections from other galaxies or related to stellar tidal streams from nearby passing galaxies.

Considering all the above, Buber et al. [35] made an open version of the HVS catalog. The public version assumes the possibility of rapid Gaia data query and automatic estimation of the posterior probability that a given star is bound to the Galaxy. Presently, the catalog includes 41 HVSs bound to the Galaxy with a probability of less than 0.5. Most objects in the catalog (32 of 41) are B-stars discovered by Brown et al. [37] in the halo survey search. The other nine stars are included in the catalog from different sources: three HVSs are from the LAMOST survey [125], one HVS, HE 0437-5439, turned out to be ejected from the Large Magellanic Cloud [128], two HVSs are related to 'hyper-runaway' stars from the disk, one HVS is the helium subdwarf US708 [124], one is the white dwarf GD429 [126], and one is the late F9 dwarf Li10 [110] mentioned above.

In summer 2019, Koposov et al. [40] discovered S5-HVS1, the first HVS in the southern hemisphere, which turned out to be the fastest HVS, with a galactocentric velocity of 1755 ± 50 km s^{-1}. It is an A star with a mass of $\sim 2.35 M_{\odot}$ located 9 kpc from the Sun. Its reconstructed trajectory uniquely points to the Galactic Center and coincides with the orbital plane of the ring disk of young stars in the nuclear cluster. The flight time of S5-HVS1 is 4.8 mln years, consistent with the cluster age, which possibly suggests their relation. This is the first example of an HVS firmly associated with the Hills mechanism. In other cases, the issue of the accuracy of the measurement of proper motion and the ejection site persists.

5.5 Problem of central ejection confirmation

HVSs were singled out as a separate class to stress their anomalous kinematics acquired from interaction with the central SMBH, as was proposed by Hills [13]. The mass scales determining momentum transfer in the Hills mechanism and the collisional stellar dynamics scenarios, including the disruption of binaries due to a supernova explosion, differ by a factor of millions. This is reflected in the HVS velocity spectrum found from modern spectroscopy with 1–3% accuracy. A high space velocity of a star is necessary but not sufficient confirmation of its origin from the Hills scenario. The ejection direction can be restored only if the tangential velocity derived from the proper motion is known. This is an astrometric problem with distant halo stars.

The first HVS catalog (MMT survey) [37] provided estimates of the theoretical proper motion components (μ_α, μ_δ) that would correspond to the ejection trajectories crossing the Galactic Center. The reconstruction of possible trajectories was done in the phase space (μ_α, μ_δ) by integrating back in time in the Galactic potential [21] from the current star location and radial velocity. The selected trajectories corresponding to a central ejection [37] predicted the proper motions of stars to be measured with the Gaia Space Telescope.

The reconstructed trajectories of 13 of 21 objects from the first HVS catalog [37] formed a sort of 'entangled' state when ejections from different parts of the disk and the Galactic Center with equal probability have the same proper motion (μ_α, μ_δ). Eight stars from the catalog [37] showed different proper motions: HVS4, HVS5, HVS6, HVS7, HVS8, HVS9, HVS10, and HVS17. This enabled the authors of [37] to conclude that at least these stars can be tested by Gaia with the announced astrometrical accuracy.

In fact, the analysis of the ejection trajectories calculated from the proper motions measured with an average error of ± 0.73 mas yr^{-1} using the Gaia DR2 showed that the ejection scenarios could be distinguished for 20 of 42 stars from the Brown review [36]. Nine stars originate in the disk, four belong to the halo, and seven are ejected from the Galactic Center: HVS1, HVS4, HVS5, HVS6, HVS9, HVS19, and HVS22. This conclusion is also supported by their measured radial velocities exceeding the second space velocity from the Galaxy at their location and by analyzing their reconstructed radial velocities at the ejection moment above 600 km s^{-1}, exceeding the parabolic speed from the stellar surface. For main-sequence B-stars with a mass of $3M_{\odot}$ and radius of $2.3R_{\odot}$, the parabolic velocity is ~ 500 km s^{-1}. This fact reliably rules out the possibility of stellar ejection from the disk due to a supernova explosion in close binaries.

A comparison of the accuracy of astronomical measurements of the proper motion by Gaia and the Hubble Space Telescope (HST) showed that Gaia errors are three times as high as those by the HST for stars fainter than 18^m. Therefore, the search for HVSs among distant halo objects is more effective by long-exposure instruments like the HST. Visible g-magnitudes for 42 stars from the survey [36] fall within the range $17^m < g < 20.25^m$, implying a Galactocentric distance interval of 25–120 kpc. The search for HVSs among disk objects is more favorable with Gaia, which provides a distance and proper motion measurement accuracy three-four times better than HST does for stars with $g < 18^m$.

Nevertheless, it is clear that advanced instrumentation with a higher angular resolution is required to increase the number of stars with anomalous kinematics, particularly to search for stars with relativistic velocities.

6. Searches for stars with relativistic velocities. Potential of modern astrometry

6.1 Search methods

There is hope that objects with relativistic velocities will be discovered in the nearest future. It is relevant to compare the situation with the direct detection of gravitational waves from coalescing binary black holes in 2015 [129]. The first experiments to detect gravitational waves started in the 1960s, although Albert Einstein predicted their existence as early as 1916. Now, decades of developing new technology seem to require a decrease in parallax and velocity measurement errors.

There are two ways to reliably estimate the velocity of a star: by measuring its proper motion and radial velocity. What is the scale of the search? From the statistics on stars with relativistic velocities, we can estimate the mean distance between them by assuming their homogeneous distribution in the Universe. For example, taking the radius of the Universe as 13.7 bln light-years, the mean distance would be ~ 30 mln light-years, or 8.7 Mpc, comparable to the distance to nearby galaxy clusters.

We should search for stars with a long lifetime ($< 1M_\odot$), which helps sustain their high velocity. But we have no spectroscopic surveys on these scales so far, and such stars are too faint for photometrical studies. So what could be some distinct features of such stars?

Depending on the star's velocity of $(1/3-2/3)c$, the relativistic factor can vary from 5 to 22%, but, spectroscopically, this effect will appear as a line shift that can be mixed with the Hubble expansion. A photometric shift depending on the color index should also occur at a level of a few tenths of the stellar magnitude. But the deviation of the trajectory of classical and relativistic objects is different [130], so, when calculating their trajectories on large spatial scales, it is essential to consider the relativistic factor. Furthermore, knowledge of these trajectories is needed to search for the ejection points of relativistic stars, which are crucial for the statistics on such objects, their spatial distribution, the mapping of their birthplaces, and further monitoring of these regions.

Relativistic stars can also appear as extended X-ray emitting bow shocks in the surrounding gas. These shocks should be visible when the star crosses intergalactic 'voids'. The ejection of the envelope by such a star ($\sim 1M_\odot$), resulting in the emergence of a 'relativistic' planetary nebula with a size significantly larger than the star, could be noticeable, which is helpful for its detection.

We stress that neutron stars, white dwarfs, and stellar-mass black holes can be accelerated to relativistic velocities much more straightforwardly than ordinary stars can. Furthermore, a neutron star at the pulsar stage will have emissions in the radio range, which may be more profitable for detection at large distances than main-sequence stars.

We also should note the ejection of a star with a planetary system, when both the star and the whole planetary system, including asteroids and comets, acquire relativistic velocities. Considering a vast population of asteroids and small bodies in planetary systems, as in the Solar System, the probability of detecting relativistic objects increases significantly. To date, we have already registered two interstellar objects: the Oumuamua asteroid [131] and the Borisov comet [132], which strengthens the existence of interstellar planets, whose number in our Galaxy is estimated as $\sim 10^{11}-10^{12}$ [133, 134].

Most likely, this is not a complete list of possible observational effects related to stars with relativistic velocities. Such stars' high kinetic energy ($\sim 10^{53}$ erg) can produce many interesting phenomena in the galaxy cluster gas.

6.2 Future space missions

The development of survey search algorithms included in the observational programs of advanced ground-based and space telescopes is very promising in the search for stars with relativistic velocities. These telescopes include JWST (James Webb Space Telescope), Euclid, WFIRST (Wide Field Infrared Survey Telescope), TMT (Thirty Meter Telescope), GMT (Giant Magellan Telescope), and Vera Rubin LSST (Large Synoptic Survey Telescope).

The launch of JWST is scheduled for November 2021 [135]. The primary tasks of this instrument include the detection of light from the first stars and galaxies that originated after the Big Bang and the detection of new planets. However, in deep surveys, mostly supergiant stars at advanced evolutionary stages of main-sequence stars with $\leqslant 1M_\odot$ will be discovered, since detecting distant, faint stars is more favorable for high-luminosity objects. The primary camera and near-infrared (0.6–5 μm) spectrograph capable of observing 100 objects in a sky area of 3×3 arcmin are appropriate for these tasks.

The next telescope is Euclid by the European Space Agency, to be launched in 2022 [136]. The primary science of this project includes the understanding of the accelerated expansion of the Universe, the search for dark energy manifestations, and its relation to GR. The operating range in the visible (550–900 nm) and near-infrared (900–2000 nm) wavelengths during a wide-field sky survey covering 15,000 square degrees up to 24^m and a deep 40 square-degree survey up to 26^m make it possible to measure several billion extragalactic sources in the program, called by the Euclid consortium (Other Science).

The WFIRST mission planned by NASA (National Aeronautics and Space Administration) in the mid-2020s will address the primary problems similar to those of the Euclid mission using a wide-field imager (WFI) equipped with a coronograph instrument (CGI) to search for exoplanets [137]. The science program includes the local and large-scale mapping of dark matter and measurements of the proper motion of stars up to 20^m with an accuracy of up to 50–125 μas yr^{-1} at a distance of about 10 kpc. The kinematic measurements will enable separating the halo stars from stellar streams produced by the tidal disruption of the Local Group dwarf galaxies or stellar clusters and improving upon the Galactic gravitational potential.

New generation telescopes, 24.5-m GMT (Giant Magellan Telescope) [138], TMT (Thirty Meter Telescope) [139], 34.5-m E-ELT (European Extremely Large Telescope) [140], are very promising. These giant ground-based facilities will have a spatial resolution ten times as high as modern telescopes, with an optical efficiency a factor of ~ 150 higher. Such telescopes will make it possible to observe the brightest stars in other galaxies, measure the light from the first galaxies, and discover new S-stars around the SMBH by measuring their velocities with an accuracy of up to 1 km s^{-1}.

In the forthcoming decade, these instruments will also start observations of stars with anomalous kinematics.

6.3 Stars with relativistic velocities as tracers of cosmological distances

Now, it is difficult to envisage what kind of new knowledge can be obtained from studying stars with relativistic velocities; however, some prospects can be delineated. For example, a star with a spatial velocity of $\sim (1/3)c$ will fly 10 pc over 100 years, go beyond the Galaxy in a million years, and cover half the distance to the Virgo cluster in a hundred million years. Even massive stars with $(2-3)M_\odot$ cannot evolve over this time and can provide information about their birthplace, including the chemical composition and kinematic features.

The motion of stars with relativistic velocities will enable studying the spatial dark matter distribution that can distort

the star's trajectory. This problem can be analyzed by choosing possible ejection trajectories by reverse integration.

The dynamics of rapidly moving stars could also help probe dark energy distribution in the Universe. Depending on the distance, the acceleration factor will change. By gradually gathering information about separate objects, it will be possible to map the relativistic 'pathways' on the scale of the Universe and to improve upon the large-scale distribution of matter.

7. Conclusion

A new class of objects with anomalously fast spatial motion with relativistic velocities will soon complete the modern kinematic classification of stars. The name reflects the possibility of limiting speeds comparable to the velocity of light. But, so far, it is a hypothetical class.

Hypervelocity stars were also initially predicted by the Hills scenario considering the dynamical capture of a binary star by the gravitational field of a supermassive black hole. They were discovered a quarter of a century later and turned out to be ordinary main-sequence stars, although hypervelocity compact objects (neutron stars, white dwarfs, and black holes) are also possible. We now know several such 'runaway' stars, actually originating after a supernova explosion in a binary system. Stars with relativistic velocities are predicted from numerical simulations of a slightly modified Hills mechanism in which one of the binary components is substituted by a second SMBH.

This substitution has a solid physical justification and is supported by numerous examples of merging galaxies and their central parts containing supermassive black holes. Nuclear stellar clusters provide a reservoir of stars for this scenario. Although stars with relativistic velocities cannot be produced in our Galaxy because of the single central SMBH, their appearance in the Universe is entirely plausible.

According to model calculations, the probability of discovering stars with a relativistic velocity is tiny, making them infrequent events. The possibility of the relativistic acceleration of stars and their planetary systems strongly enhances their detection probability. The discovery of interstellar objects such as the CNEOS 2014-01-08 meteor [141], Oumuamua asteroid [131], and Borisov comet [132] gives hope in the search for traces of interstellar objects in the Solar System. Such searches could be started by detailed studies of the lunar surface pocked with craters, evidencing previous asteroid activity.

Siraj and Loeb [142] propose a project for a telescope in the lunar orbit capable of registering meteor events. On Earth, meteors are burned away in the atmosphere; on the Moon, they leave traces that become more noticeable as the velocity rises. The lunar telescope could continuously watch the intensity of optical flares from which the crater size could be inferred. Among such flares, some could be due to interstellar meteors with higher velocities than small bodies (asteroids) in the Solar System. Paper [142] gives the formula relating the crater diameter and energy released during impact, in which the mass and velocity are unified as energy. The lunar telescope envisions spectroscopic measurements following the flares to analyze in detail the composition of the impact particles, which can be used to distinguish their origin as being from the Solar System or as interstellar. Moreover, the spectrum will bear information on the specific impact energy independent of the mass, being characterized solely by the impact velocity. A detailed physical analysis of the interaction of a relativistic meteor with the lunar surface is required to find specific features of super-high velocities.

Besides the Moon, the 'archaeological' deciphering of traces of relativistic impacts can also be performed for other Solar System bodies (Mercury, Mars, giant planet satellites, etc.).

We can definitely state that the scenarios generating stars with relativistic velocities do not contradict the laws of nature, and the discovery of such objects is a matter of time.

References

1. Curtis H D *Bull. Natl. Res. Council* **2** 171 (1921)
2. Shapley H *Bull. Natl. Res. Council* **2** 194 (1921)
3. Kapteyn J C, Kapteyn W *Publ. Kapteyn Astron. Lab. Groningen* **5** 1 – 87 (1900)
4. Lindblad B *Arkiv Mat. Astron. Fys.* **23A** (18) 12 (1933)
5. Oort J H *Bull. Astron. Inst. Netherlands* **4** 269 (1928)
6. Baade W *Sci. Am.* **195** (3) 92 (1956)
7. Zwicky F *Morphological Astronomy* (Berlin: Springer, 1957)
8. Peri C S et al. *Rev. Mexicana Astron. Astrofis. Conf.* **40** 156 (2011)
9. Cordes J M, Romani R W, Lundgren S C *Nature* **362** 133 (1993)
10. Lacy J H, Achtermann J M, Serabyn E *Astrophys. J. Lett.* **380** L71 (1991)
11. McGinn M T et al., in *Infrared Spectroscopy in Astronomy. Proc. of the 22nd Eslab Symp., Salamanca, Spain, 7 – 9 December 1988* (European Space Agency Special Publ., Vol. 290, Ed. B H Kaldeich) (Paris: European Space Agency, 1989) p. 421
12. Eckart A, Genzel R *Nature* **383** 415 (1996)
13. Hills J G *Nature* **331** 687 (1988)
14. Schödel R et al. *Astrophys. J.* **596** 1015 (2003)
15. Brown W et al. *Astrophys. J.* **622** L33 (2005)
16. Gualandris A, Zwart S P, Sipior M S *Mon. Not. R. Astron. Soc.* **363** 223 (2005)
17. Bromley B C et al. *Astrophys. J.* **653** 1194 (2006)
18. Baumgardt H, Gualandris A, Zwart S P *Mon. Not. R. Astron. Soc.* **372** 174 (2006)
19. O'Leary R M, Loeb A *Mon. Not. R. Astron. Soc.* **383** 86 (2008)
20. Sherwin B D, Loeb B, O'Leary R M *Mon. Not. R. Astron. Soc.* **386** 1179 (2008)
21. Kenyon S J et al. *Astrophys. J.***680** 312 (2008)
22. Abadi M G, Navarro J F, Steinmetz M *Astrophys. J.* **691** L63 (2009)
23. Zubovas K, Wynn G A, Gualandris A *Astrophys. J.* **771** 118 (2013)
24. Šubr L, Haas J *Astrophys. J.* **786** 121 (2014)
25. Capuzzo-Dolcetta R, Fragione G *Mon. Not. R. Astron. Soc.* **454** 2677 (2015)
26. Dremova G N, Dremov V V, Tutukov A V *Astron. Rep.* **58** 291 (2014); *Astron. Zh.* **91** 353 (2014)
27. Wu X et al. *Mon. Not. R. Astron. Soc.* **386** 2199 (2008)
28. Miralda-Escudé J, Gould A *Astrophys. J.* **545** 847 (2000)
29. Sesana A, Haardt F, Madau P *Astrophys. J.* **660** 546 (2007)
30. Chandrasekhar S *Astrophys. J.* **97** 255 (1943)
31. Gillessen S, in *Intern. Workshop Modest-13, Star Clusters Across Cosmic Time, Almaty, Kazakhstan, August 19 – 23, 2013. Abstracts* (Almaty: Fesenkov Astrophysical Institute, 2013) p. 23; http://aphi.kz/wp-content/uploads/2015/07/MODEST-13-Booklet.pdf
32. Ghez A M et al. *Astrophys. J.* **620** 744 (2005)
33. Eisenhauer F et al. *Astrophys. J.* **628** 246 (2005)
34. Gillessen S et al. *Astrophys. J.* **837** 30 (2017)
35. Boubert D et al. *Mon. Not. R. Astron. Soc.* **479** 2789 (2018)
36. Brown W R et al. *Astrophys. J.* **866** 39 (2018)
37. Brown W, Geller M J, Kenyon S J *Astrophys. J.* **787** 89 (2014)
38. Capuzzo-Dolcetta R, Fragione G *Mon. Not. R. Astron. Soc.* **454** 2677 (2015)
39. Marchetti T et al. *Mon. Not. R. Astron. Soc.* **470** 1388 (2017)
40. Koposov S E et al. *Mon. Not. R. Astron. Soc.* **491** 2465 (2020)
41. Guillochon J, Loeb A *Astrophys. J.* **806** 124 (2015)
42. Dremova G N, Dremov V V, Tutukov A V *Astron. Rep.* **61** 573 (2017); *Astron. Zh.* **94** 580 (2017)
43. Schödel R et al. *Nature* **419** 694 (2002)

44. Ren J et al. *Mon. Not. R. Astron. Soc.* **499** 3399 (2020)
45. Dryomova G N, Dryomov V V, Tutukov A V *Astron. Rep.* **62** 971 (2018); *Astron. Zh.* **95** 867 (2018)
46. Blaauw A *Bull. Astron. Inst. Netherlands* **15** 265 (1961)
47. Poveda A, Ruiz J, Allen C *Boletin Observ. Tonantzintla Tacubaya* **4** 86 (1967)
48. Napiwotzki R, Silva D V *Memorie Soc. Astron. Italiana* **83** 272 (2012); arXiv:1109.4116
49. Heber E et al. *Astron. Astrophys.* **483** L21 (2008)
50. Lynden-Bell D, Rees M J *Mon. Not. R. Astron. Soc.* **152** 461 (1971)
51. Kilic M et al. *Mon. Not. R. Astron. Soc.* **434** 3582 (2013)
52. Tutukov A V, Fedorova A V *Astron. Rep.* **53** 839 (2009); *Astron. Zh.* **86** 902 (2009)
53. Bardeen J M, Press W H, Teukolsky S A *Astrophys. J.* **178** 347 (1972)
54. Yu Q, Tremaine S *Astrophys. J.* **599** 1129 (2003)
55. Dremova G N et al. *Astron. Rep.* **59** 1019 (2015); *Astron. Zh.* **92** 907 (2015)
56. Verlet L, Weis J-J *Phys. Rev. A* **5** 939 (1972)
57. Fellhauer M et al. *Astrophys. J.* **651** 167 (2006)
58. Carter B, Luminet J P *Mon. Not. R. Astron. Soc.* **212** 23 (1985)
59. Lynden-Bell D *Nature* **223** 690 (1969)
60. Dokuchaev V I, Ozernoi L M *Sov. Astron. Lett.* **3** 209 (1977); *Pis'ma Astron. Zh.* **3** 391 (1977)
61. Miles P, Coughlin E, Nixon C *Astrophys. J.* **899** 36 (2020)
62. Mainetti D et al. *Astron. Astrophys.* **600** A124 (2017)
63. Ivanov P B, Novikov I D *Astrophys. J.* **549** 467 (2001)
64. Guillochon J, Ramirez-Ruiz E *Astrophys. J.* **767** 25 (2013)
65. Dryomova G, Dryomov V, Tutukov A *Baltic Astron.* **24** 1 (2015)
66. Dremova G N, Dremov V V, Tutukov A V *Astron. Rep.* **60** 695 (2016); *Astron. Zh.* **93** 685 (2016)
67. Sofue Y, Rubin V *Annu. Rev. Astron. Astrophys.* **39** 137 (2001)
68. Dremova G N, Dremov V V, Tutukov A V *Astron. Rep.* **63** 862 (2019); *Astron. Zh.* **96** 866 (2019)
69. Loose H H, Krügel E, Tutukov A *Astron. Astrophys.* **105** 342 (1982)
70. Fragione G, Capuzzo-Dolcetta R, Kroupa P *Mon. Not. R. Astron. Soc.* **467** 451 (2017)
71. Shipp N et al. (DES Collab.) *Am. Astron. Soc. AAS Meeting* **231** (231) 212.05 (2018)
72. Iben I (Jr.), Tutukov A V *Astrophys. J.* **284** 719 (1984)
73. Popova E I, Tutukov A V, Yungelson L R *Astrophys. Space Sci.* **88** 55 (1982)
74. Svechnikov M A et al. *Nauch. Inform.* **67** 15 (1989)
75. Duquennoy A, Mayor M *Astron. Astrophys.* **248** 485 (1991)
76. Kobulnicky H, Fryer C *Astron. Astrophys.* **670** 747 (2007)
77. Kraicheva Z T et al. *Sov. Astron.* **22** 670 (1978); *Astron. Zh.* **55** 1176 (1978)
78. Scalo J M, in *Protostars and Planets II* (Eds D C Black, M S Matthews) (Tucson, AZ: Univ. Arizona Press, 1985) p. 201
79. Svechnikov M A *Issledovanie Effektov Vzaimodeistviya v Tesnykh Dvoinykh Sistemakh s Nerelyativistskimi Komponentami* (Study of Effects of Interaction in Close Binaries with Nonrelativistic Components) (Tallin: Valgus, 1990) p. 26
80. Salpeter E E *Astrophys. J.* **121** 161 (1955)
81. Kroupa P *Mon. Not. R. Astron. Soc.* **322** 231 (2001)
82. Perets H B *Astrophys. J.* **690** 795 (2009)
83. Aharon D, Battistu A M, Perets H B *Astrophys. J.* **823** 137 (2016)
84. Lacy J et al. *Astrophys. J.* **241** 132 (1980)
85. Fridman A M, Yanchenko S G *Astron. Rep.* **53** 969 (2009); *Astron. Zh.* **86** 1043 (2009)
86. Plewa P et al. *Mon. Not. R. Astron. Soc.* **453** 3234 (2015)
87. Chatzopoulos S et al. *Mon. Not. R. Astron. Soc.* **447** 948 (2015)
88. Gillessen S et al. *The Messenger* (120) 26 (2005)
89. Gillessen S et al. *Astrophys. J.* **692** 1075 (2009)
90. Ghez A M et al. *Astrophys. J.* **689** 1044 (2008)
91. Abuter R et al. (GRAVITY Collab.) *Astron. Astrophys.* **615** L15 (2018)
92. Peiβker F, Eckart A, Parsa M *Astrophys. J.* **889** 61 (2020)
93. Parsa M et al. *Astrophys. J.* **845** 22 (2017)
94. Bambi C *Phys. Rev. D* **83** 103003 (2011)
95. Akiyama K et al. (The Event Horizon Telescope Collab.) *Astrophys. J. Lett.* **875** L1 (2019)
96. Amorim A et al. (GRAVITY Collab.) *Phys. Rev. Lett.* **122** 101102 (2019)
97. Balick B, Brown R L *Astrophys. J.* **194** 265 (1974)
98. Abuter R et al. (The GRAVITY Collab.) *Astron. Astrophys.* **625** L10 (2019)
99. Gillessen S et al. *Astrophys. J.* **871** 126 (2019)
100. Bower G C et al. *Astrophys. J.* **588** 331 (2003)
101. Baganoff F K et al. *Astrophys. J.* **591** 891 (2003)
102. Falcke H et al. *Astrophys. J.* **499** 731 (1998)
103. von Fellenberg S D et al. *Astrophys. J.* **862** 129 (2018)
104. Gunn J E et al. *Astron. J.* **131** 2332 (2006)
105. Yanny B et al. *Astrophys. J.* **540** 825 (2000)
106. Fukugita M et al. *Astrophys. J.* **111** 174 (1996)
107. Brown W R et al. *Astrophys. J.* **647** 303 (2006)
108. Yanny B et al. *Astrophys. J.* **137** 4377 (2009)
109. Palladino L E et al. *Astrophys. J.* **780** 7 (2014)
110. Li Y-B et al. *Res. Astron. Astrophys.* **15** 1364 (2015)
111. Cui X-Q et al. *Res. Astron. Astrophys.* **12** 1197 (2012)
112. Munn J A et al. *Astron. J.* **136** 895 (2008)
113. Aihara H et al. *Astrophys. J. Suppl.* **193** 29 (2011)
114. Castelli F, Kurucz R L, astro-ph/0405087
115. Brown W R, Geller M J, Kenyon S J *Astrophys. J.* **751** 55 (2012)
116. Lu Y, Zhang F, Yu Q *Astrophys. J.* **709** 1356 (2010)
117. Arenou F et al. *Astron. Astrophys.* **599** A50 (2017)
118. Luri X et al. *Astron. Astrophys.* **616** A9 (2018)
119. Katz D et al. (Gaia Collab.) *Astron. Astrophys.* **616** A11 (2018)
120. Antoja T et al. *Nature* **561** 360 (2018)
121. Bovy J *Astrophys. J. Suppl.* **216** 29 (2015)
122. Marchetti T, Rossi E M, Brown A G A *Mon. Not. R. Astron. Soc.* **490** 157 (2019)
123. Hirsch H A et al. *Astron. Astrophys.* **444** L61 (2005)
124. Justham S et al. *Astron. Astrophys.* **493** 1081 (2009)
125. Geier S et al. *Science* **347** 1126 (2015)
126. Vennes S et al. *Science* **357** 680 (2017)
127. Raddi R et al. *Mon. Not. R. Astron. Soc.* **479** L96 (2018)
128. Edelmann H et al. *Astrophys. J.* **634** L181 (2005)
129. Abbott B P et al. (LIGO Scientific Collab. and Virgo Collab.) *Phys. Rev. Lett.* **116** 131102 (2016)
130. Barrabès C, Hogan P A *Class. Quantum Grav.* **21** 405 (2003)
131. Rice M, Laughlin G *Astrophys. J. Lett.* **884** L22 (2019)
132. Guzik P et al. *Nat. Astron.* **4** 53 (2020)
133. Clanton C, Gaudi B S *Astrophys. J.* **834** 46 (2017)
134. Burgasser A et al., in *Protostars and Planets V* (Eds B Reipurth, D Jewitt, K Keil) (Tucson, AZ: Univ. Arizona Press, 2007) p. 951
135. NASA. James Webb Space Telescope, https://www.jwst.nasa.gov
136. Euclid Consortium, https://www.euclid-ec.org/
137. NASA. Nancy Grace Roman Space Telescope, https://roman.gsfc.nasa.gov/about.html
138. Giant Magellan Telescope, https://www.gmto.org/
139. Thirty Meter Telescope International Observatory, https://www.tmt.org
140. European Southern Observatory. Extremely large telescopes, https://www.eso.org/public/teles-instr/elt
141. Siraj A, Loeb A *Astrophys. J. Lett.* **872** L10 (2019); arXiv: 1906.03270
142. Siraj A, Loeb A *Acta Astronautica* **173** 53 (2020)